

Patupilone-induced apoptosis is mediated by mitochondrial reactive oxygen species through Bim relocation to mitochondria.

Khawaja NR, Carré M, Kovacic H, Estève MA, Braguer D.

INSERM UMR911, Centre de Recherche en Oncologie biologique et Oncopharmacologie;
Université Aix-Marseille, France.

Running title: Mitochondrial ROS–mediated Bim relocalization and apoptosis.

Corresponding author: Pr. Diane. Braguer, INSERM UMR911, Faculté de Pharmacie, 27
Bd Jean Moulin, 13385 Marseille Cedex 05, France.

Phone : +33-4-91-83-56-35

Fax : +33-4-91-83-56-35

E-mail: diane.braguer@univmed.fr

Number of text pages 29

Number of tables: 0

Number of figures 09

Number of references: 41

Number of words in abstract: 249

Number of words in introduction: 628

Number of words in discussion: 894

Abbreviations: P-gp, P-glycoprotein; MTAs, microtubule-targeted agents; MTT, 3-(4,5-dimethylthiazol-2-yl)-2,5-diphenyltetrazolium bromide; FITC, fluoresceine iso thio cyanate; DAPI, 4',6-diamidino-2-phenylindole; DiOC₆, 3,3'-dihexyloxacarboxyanine iodide; $\Delta\Psi_m$, mitochondrial membrane potential; MDR, multidrug resistance; DMSO, dimethylsulfoxide; DCF-DA, dichlorofluorescein diacetate; PI, propidium iodide; VDAC, voltage-dependent anion channel; MOMP, mitochondrial outer membrane permeabilization; ROS, reactive oxygen species; COX II, Cytochrome c oxidase II.

ABSTRACT

Among the new microtubule-targeted agents, the Epothilone family of molecules has shown promising anti-cancer potential, and clinical trials are currently under way for patupilone (epothilone B) in various cancer indications. In this study, we characterized novel aspects of patupilone's cellular action that may underly its potent cytotoxicity in human neuroblastoma cells. Patupilone induced mitochondrial membrane potential collapse, mitochondrial morphological changes and cytochrome c release, leading to apoptosis. Within the two first hours, patupilone increased generation of reactive oxygen species (ROS), *i.e.* superoxides and hydrogen peroxide ($33 \pm 6\%$ and $51 \pm 3\%$ increase respectively), specifically from mitochondria. ROS scavengers and mitochondrial DNA depletion (p^{-} cells) significantly protected cells against patupilone cytotoxicity, indicating that ROS generation is a key event in the initial phase of apoptosis. While Bim expression level was not modified by patupilone, this pro-apoptotic protein accumulated in the mitochondrial compartment (2.4 fold increase at IC_{70}) after only a 6 hr-treatment. In contrast, Bax and Bcl-2 mitochondrial levels were not changed during treatment. Importantly, ROS inhibition prevented Bim relocalization to mitochondria and mitochondrial membrane changes induced by patupilone. Altogether, our data reveal that patupilone-mediated ROS production by mitochondria initiates the intrinsic signaling cascade by inducing Bim accumulation in mitochondria. These results might explain the superior activity of patupilone in tumor cells as compared with paclitaxel that is, until now, the clinical reference among microtubule-stabilizing agents. Furthermore, our data highlight the importance of mitochondria that simultaneously assume the role of activator and integrator of apoptotic signals triggered by patupilone.

INTRODUCTION

Microtubules play a basic role in diverse cellular functions including cell division and trafficking of intracellular organelles, vesicles and proteins. They are very dynamic structures and are referred as successful targets for microtubule-targeted agents (MTAs) in cancer chemotherapy (Jordan and Kamath, 2007). MTAs suppress microtubule dynamics in tumour cells, which generally results in impairment of both mitotic and interphasic networks (Pasquier et al., 2006). These drugs are also potent inducers of apoptosis, a complex programmed-cell death process that involves intrinsic signalling cascades converging to mitochondria (Pourroy et al., 2004).

Among MTAs, taxanes are microtubule-stabilizing agents, which are widely used in cancer therapy. Despite their demonstrated effectiveness, their clinical success has been severely hindered by the emergence of resistant tumor cells. Acquired resistance can result from the enhanced expression of P-glycoprotein (P-gp), tubulin mutations or changes in microtubule subtypes composition, and alterations in apoptotic signalling pathways (Ferlini et al., 2003; Orr et al., 2003; Sève et al., 2007). These limitations have led to an intensive search for new microtubule-stabilizing agents, which resulted in isolation of the epothilone family of molecules from myxobacterium *Sorangium cellulosum*. Among them, patupilone (epothilone B, EPO906) has shown a promising anti-cancer activity *in vitro* and *in vivo*, and is currently undergoing phase III clinical trials. Interestingly, epothilones are active against P-gp overexpressing cancer cells resistant to paclitaxel (Taxol[®]) (Altmann et al., 2007). Elsewhere, while epothilones bind to the same β -tubulin site as taxanes (Bollag et al., 1995; Nettles et al., 2004), they remain active against cells and xenograft models that have developed resistance to taxanes as a result of tubulin subtypes mutations or overexpression (Nicolaou et al., 1997; Lee

et al., 2008) In addition, the microtubule-stabilizing activity of epothilones is not always related to their anti-tumor effectiveness (Nicolaou et al., 1997). Thus, other cellular targets and specific mechanisms of action may exist for this new class of MTAs.

Mitochondria are essential cellular organelles for ATP synthesis, reactive oxygen species (ROS) homeostasis and apoptosis orchestration (Newmeyer et al., 2003). Their central role in apoptosis induction by MTAs is now uncontested (Estève et al., 2007). Disruption of the mitochondrial membrane potential ($\Delta\Psi_m$) and release of death promoting factors like cytochrome c are critical pro-apoptotic events, which are largely reported to be controlled by the Bcl-2 family of proteins (Adams and Cory, 2007). The relative levels of pro- and anti-apoptotic members of the Bcl-2 family, localized in the mitochondrial compartment, determine the cell susceptibility to apoptosis. Interestingly, variations in cell sensitivity to paclitaxel have been related to Bim expression levels (Putchá et al., 2001; Li et al., 2005; Li et al., 2007). Without apoptotic stimulus, Bim may be sequestered in the microtubule cytoskeleton through its binding to dynein motor complexes (Puthalakath et al., 1999). However, no evidence exists regarding Bim relocalization during apoptosis induced by microtubule-stabilizing agents.

Mitochondrial respiratory chain complexes are key sources of reactive oxygen species (ROS), well-known mediators of various biological responses (Archer et al., 2008). It has been shown that paclitaxel enhanced ROS production from both mitochondria and NADPH oxidase (Varbiro et al., 2001; André et al., 2002; Alexandre et al., 2006). Moreover, anti-oxidants protected cells against apoptosis induced by docetaxel, indicating that ROS accumulation could contribute to the cell death process induced by microtubule-stabilizing agents (Taniguchi et al., 2005). However, the early apoptotic route induced by MTA-mediated mitochondrial ROS generation in cancer cells has not been explored yet.

In this study, we showed that early ROS production from mitochondria plays an important role in the onset of patupilone-induced apoptosis, through modifications in mitochondrial membrane permeability. Indeed, this is the first study showing that ROS generated by mitochondria mediates, in turn, Bim relocalization to mitochondria. We thus characterized novel aspects of patupilone's cellular action that may underly its potent growth inhibition of human tumor cells.

MATERIALS AND METHODS

Drugs and reagents. Patupilone (epothilone B) and epothilone A were kindly provided by Dr. M. Wartmann (Novartis Pharma AG, Basel, Switzerland) as pure substances and were dissolved in DMSO to obtain stock solutions. Stock solutions of WST-1 (2-(4-Iodophenyl)-3-(4-nitrophenyl)-5-(2, 4-disulfophenyl)-2H) (Interchim, Montluçon, France), DCF-DA (Molecular Probes, Eugene, Oregon), lucigenin, NADPH, allopurinol and rotenone (Sigma, Saint Louis, MO) were dissolved in DMSO. Potassium cyanide (KCN), tiron (4, 5-dihydroxybenzene-1, 3-disulfonic acid disodium salt) (Sigma) were prepared in sterile water and sodium pyruvate was purchased from Gibco, Grand Island, NY.

Cell culture and drug treatment. Human neuroblastoma SK-N-SH and IMR-32 cells were routinely maintained in culture medium according to standard procedures (Pourroy et al., 2004; André N al., 2000). 37×10^3 cells/cm² were seeded 72 hr before treatment. For co-incubation experiments, tiron was added at 2 mM, sodium pyruvate at 10 mM, allopurinol (3,5,7,8-tetraazabicyclo[4.3.0] nona-3,5,9-trien-2) at 500 μ M, rotenone [1,2,12,12a-tetrahydro-8,9-dimethoxy-2-(1-methylethenyl-(1)benzopyrano (2,4-b) furo (2,3-h)(1) benzopyran-6 (6H)] at 100 nM and KCN (potassium cyanide) at 100 μ M. Rho negative (ρ^{-}) SK-N-SH cells were obtained by incubating SK-N-SH cells for 8 weeks with routine culture medium supplemented with 100 ng/ml ethidium bromide (EtBr, 2,7-diamino-9-phenyl-10-ethyl phenanthridinium bromide) sodium pyruvate (1 mM), uridine (50 μ g/ml), and glucose (4.7 mg/ml) (Patenaude et al., 2007). These cells were then maintained in same culture medium without ethidium bromide.

Cytotoxicity assay. Growth inhibition of neuroblastoma cells and ρ^{-} was studied following a 72 hr treatment with drugs by using the MTT cell proliferation assay (Pourroy et al., 2004; Estève et al., 2006). For short exposure treatments, after specific treatment duration (6 hr or 24 hr) culture medium with drug was replaced by normal culture medium and MTT assay was

performed at 72 hr after treatment. While comparing the impact of patupilone on $\rho^{(+)}$ and $\rho^{(-)}$ SK-N-SH, seeding and treatment schedule of respective cells was designed in a manner that cell confluence was identical during treatment. P-gp was completely inhibited by 10 μ M of verapamil, as we previously determined (Estève et al., 2006). At least three independent experiments (in quadruplicate) were performed for each respective condition.

Flow cytometry. SK-N-SH cells were fixed, permeabilized and stained with propidium iodide as previously described (Pourroy et al., 2004; Estève et al., 2006). Measurement of fluorescence was performed by flow cytometry (FACScan, Beckton Dickinson). Results obtained were analysed by Cell Quest Pro software. At least three independent experiments were performed for each condition.

Fluorescent microscopy. Cells were grown on 8 well plates and incubated with drugs for 48 hr. Cells were then fixed with 3.7% formaldehyde, permeabilized with 1% saponine and successively incubated with the anti-cytochrome c antibody (Pharmingen, San Diego, CA) and a secondary antibody conjugated with FITC (Jackson Immunosearch, West Grove, PA) as previously described (Pourroy et al., 2004; Estève et al., 2006). For nuclei visualization, cells were additionally stained with DAPI. Cells were observed using a Leica DM-IRBE microscope coupled with a digital camera (CCD camera cool snapFX; Princeton Instruments) and results were analysed with Metamorph software (Universal Imaging Corporation, Downingtown, PA).

Mitochondria isolation and Western blotting. Mitochondria were isolated from treated SK-N-SH cells as we previously described (André et al., 2000). Equal amounts of proteins from mitochondrial pellets or whole cells were separated by SDS-PAGE and electrotransferred onto a nitrocellulose membrane. Primary antibodies used were directed against p53 and COX II (Santa Cruz Biotechnology, CA), p21/WAF1 (Oncogene Research Product, San Diego, CA),

Bim, Bak and Bax (Santa Cruz Biotechnology), Bcl-2 (Dako cytometry, Denmark), cytochrome c (Pharmingen), VDAC and α -tubulin (Sigma, St Louis, MO). Peroxydase-conjugated goat anti-mouse, donkey anti-rabbit antibodies (Jackson Immunosearch) and donkey anti-goat (Santa Cruz Biotechnology) were used as secondary antibodies. Visualization was accomplished using an enhanced chemiluminescence detection kit (Amersham Biosciences, Piscataway). Protein quantification of blots was performed by using Image J software. Three independent experiments were performed.

Electron microscopy. After treatment with patupilone IC₇₀ and/or tiron, cells were fixed with 2.5 % glutaraldehyde for 10 min. Then, cells were scratched mechanically, dehydrated in ethanol, embedded in Epon, and cut into thin sections as previously described (André et al., 2002). The samples were imaged by a transmission electron microscope (JEOL 1220). At least 200 mitochondria were analyzed in three independent experiments (IPS Samba Technologies, Grenoble, France).

Measurement of reactive oxygen species. Superoxide ions generation was measured either by WST-1 colorimetric test or lucigenin chemiluminescence. Cells were treated, in 96 well plates, with patupilone and ROS scavengers/inhibitors before incubation with WST-1 (500 μ M) for 30 min. For the chemiluminescence test, cells were suspended in a solution containing lucigenin (0.3 mg/ml) and NADPH (17 mg/ml) during 2 hr treatment (Morazzani et al., 2004). Hydrogen peroxide production was evaluated by H₂-DCFDA fluorescence as described (Morazzani et al., 2004). Concentration of H₂-DCFDA used, was extended to 100 μ M in our conditions. Lucigenin and H₂-DCFDA ROS measurements were both performed using a Fluoroskan Ascent FL plate reader (Labsystems, France), and WST-1 measurements with Labsystems Multiscan RC (Honoré et al., 2003). All measurements were performed at 37°C.

Statistical analysis. Results are expressed as means \pm SD from at least 3 independent experiments. Statistical analysis was done using Student's test. The value of $p < 0.05$ was considered statistically significant.

RESULTS

Patupilone potently induces apoptosis in human neuroblastoma cells, regardless of the multidrug resistance status.

We first determined that patupilone inhibited SK-N-SH cell growth at low nanomolar concentrations (Figure 1A-B). After a 72 hr-treatment, the IC_{50} value –concentration that inhibits 50% of cell growth – was only 1.88 nM. Epothilone A was considerably less active than patupilone, since its IC_{50} reached 70 nM. Patupilone was also 50 times more potent in SK-N-SH cells than paclitaxel ($IC_{50} = 100$ nM), which is the clinical reference compound among microtubule-stabilizing agents (Figure 1A-B). Interestingly, 6 hr as well as 24 hr exposure of cells with patupilone induced the same level of cytotoxicity as a 72 hr of drug exposure ($p > 0.05$, Figure 1C) indicating that early patupilone effects were sufficient for its activity. During patupilone treatment, a marked fraction of the population of cells displayed apoptotic characteristics (nuclei fragmentation and sub-G1 cells) (Figure 2A-B).

In contrast to the taxanes and other MTAs, patupilone has been reported not to be subject to P-gp mediated drug efflux. Here, we found that patupilone was as active in the P-gp overexpressing cells SK-N-SH ($IC_{50} = 1.9 \pm 0.3$ nM) as in the P-gp negative ones IMR-32 ($IC_{50} = 1.4 \pm 0.5$ nM, $p > 0.05$) (data not shown). Inhibition of P-gp by verapamil did not modify patupilone cytotoxicity in SK-N-SH cells, confirming that patupilone is not a substrate of P-gp (Figure 2C). In sharp contrast, P-gp inhibition increased paclitaxel cytotoxicity in SK-N-SH cells (100 nM became IC_{80}), but it remained insufficient to render it as potent as patupilone ($IC_{80} = 5.5$ nM) (Figure. 2C). Lastly, paclitaxel was also significantly less active than patupilone in P-gp negative IMR-32 cells ($IC_{50} = 6.3 \pm 0.3$ nM and 1.4 ± 0.5 nM respectively, $p < 0.01$). Thus, the difference in cell sensitivity to these MTAs was probably not only due to the P-gp status of neuroblastoma cells, but might be due to enhanced patupilone's ability to activate apoptotic signals.

Patupilone alters mitochondria function and morphology.

To determine whether patupilone activates the intrinsic apoptosis pathway, we first measured the mitochondrial membrane potential variations from 2hr to 24 hr treatment (Figure 3A). At 6 hr of treatment with IC_{70} of patupilone, mitochondrial membrane depolarization was observed (38 ± 4 % decrease in $DIOC_6$ uptake; $p < 0.05$). After a 24 hr-treatment, the membrane potential collapse was not amplified ($p > 0.05$ as compared with 6 hr) indicating that patupilone induced maximal changes in mitochondrial membrane integrity as soon as 6 hr of treatment. We then studied whether mitochondrial membrane depolarization was associated with the release of pro-apoptotic factors from the intermembrane space. Therefore, we isolated mitochondria from control and patupilone-treated cells (IC_{70}). Cytochrome c confined in mitochondria was reduced by 66 ± 2 % after only 6 hr of treatment, and the maximum reduction was achieved at 24 hr (83 ± 1 %)(Figure 3B). Cytochrome c relocalization was also confirmed by fluorescent microscopy after cell treatment (IC_{70}) for 24 hr. Punctuated staining in control cells indicated the presence of cytochrome c in intact mitochondria, whereas the diffused fluorescence in treated cells gave evidence of its release in the cytosol (Figure 3C). Thus, these observations indicate that patupilone induces neuroblastoma cell death by early disrupting the mitochondrial membrane potential, followed by cytochrome c release.

We previously showed that apoptosis induced by microtubule-stabilizing agents in neuroblastoma cells can be associated with early changes in mitochondria structure (André et al., 2002). Hence, we evaluated patupilone impact on mitochondria morphology. As shown by electron microscopy (Figure 4), patupilone (IC_{70}) early increased cristae surface (6 hr), modifying the appearance of mitochondria to a “striped” phenotype. In treated cells, 75 ± 3 % of mitochondria were affected, while it was restricted to a minority in control cells (3 ± 1 %).

This change in structure was maintained after a 20-hr treatment with patupilone for 76 ± 4 % of mitochondria. The swelling and the subsequent non-specific rupture of mitochondrial membrane only occurred later, affecting 20 ± 3 % of mitochondria at 40 hr, versus 4 % in control cells. Altogether, these results show that patupilone early affects the mitochondrial membrane integrity, inducing both morphological and permeability changes.

Increase in reactive oxygen species specifically generated by mitochondria mediates patupilone cytotoxicity.

In addition to the established role of mitochondria as reservoir for pro-apoptotic factors, the mitochondrial compartment constitutes an important generator of ROS. Then, using the WST-1 assay, we first measured $O_2^{\circ-}$ levels during patupilone treatment. As shown in figure 5A, the drug promoted $O_2^{\circ-}$ production in a concentration-dependent manner. The kinetic analysis of this production revealed a significant increase within the two first hours of treatment (33 ± 6 % increase for IC_{90}), which was maintained up to 24 hr. This early effect of patupilone was confirmed by measuring $O_2^{\circ-}$ by using the lucigenin assay, with a 69 ± 4 % increase ($p < 0.01$) for IC_{50} after only 30 min. In parallel, H_2O_2 levels were detected by the DCF-DA test. As observed for $O_2^{\circ-}$, patupilone (IC_{90}) rapidly enhanced H_2O_2 formation by 51 ± 3 % at 2 hr, 32 ± 7 % at 6 hr (Figure 5B) and 47 ± 5 % at 24 hr (data not shown).

To determine whether the ROS produced were of mitochondrial origin, we co-incubated cells with patupilone and rotenone or potassium cyanide (KCN), inhibitors of mitochondrial electron transport chain complexes. Importantly, patupilone-mediated increase in H_2O_2 levels was prevented by both rotenone and KCN (Figure 5B). Similarly, rotenone inhibited $O_2^{\circ-}$ production induced by patupilone (Figure 5C). In contrast, allopurinol that inhibits xanthine oxidase, a cytosolic source for cellular $O_2^{\circ-}$, did not inhibit the patupilone-induced ROS production (Figure 5B). Thus, patupilone specifically enhanced ROS generation from mitochondria. Lastly, sodium pyruvate (H_2O_2 scavenger) was as potent as tiron ($O_2^{\circ-}$

scavenger) in inhibiting H_2O_2 increase (Figure 5B), strongly suggesting that the mitochondrial H_2O_2 resulted from $\text{O}_2^{\circ-}$ dismutation.

To further demonstrate the mitochondrial origin of ROS, we compared ROS production induced by patupilone in wild type SK-N-SH cells, *i.e.* $\rho^{(+)}$, and SK-N-SH cells that were partially depleted of mitochondrial DNA, *i.e.* $\rho^{(-)}$. $\rho^{(-)}$ cells were characterized by a strong inhibition of the mitochondrial energy production, as indicated by the incapacity to grow in glucose-deprived medium (data not shown). These cells do not express essential components of the mitochondrial respiratory chain, as confirmed by the 76 ± 1 % decrease in cytochrome c oxidase II (COX II) expression, a mitochondrial DNA-encoded protein (Figure 6A). In contrast with $\rho^{(+)}$ SK-N-SH cells, patupilone did not trigger $\text{O}_2^{\circ-}$ generation in $\rho^{(-)}$ cells (Figure 5C), confirming ROS were specifically produced by mitochondria.

To investigate whether mitochondrial ROS were involved in patupilone efficacy, we measured the cytotoxicity of patupilone in $\rho^{(-)}$ cells. Interestingly, $\rho^{(-)}$ cells were markedly resistant to patupilone as compared with $\rho^{(+)}$ cells (Figure 7A). For example, cell survival at IC_{70} (5 nM) was increased from 27 ± 4 % in $\rho^{(+)}$ SK-N-SH cells to 59 ± 6 % in $\rho^{(-)}$ cells ($p < 0.05$). Since expression of nuclear DNA-encoded proteins of the apoptotic machinery (cytochrome c, Bcl-2, Bim and Bax) remained intact in $\rho^{(-)}$ cells (Figure 6B), mitochondrial ROS abrogation was responsible for $\rho^{(-)}$ cell resistance to patupilone. Then, we confirmed these results by using tiron and sodium pyruvate in wild type SK-N-SH cells. As observed in $\rho^{(-)}$ cells, both anti-oxidants considerably protected cells against patupilone cytotoxic effects when added from the beginning of treatment (Figure 7B-C). In combination with patupilone IC_{70} , tiron increased cell survival from 32 ± 1 % to 71 ± 2 % ($p < 0.05$). Moreover, the IC_{50} value, which was 2 nM for patupilone alone, strongly increased in presence of tiron and was even not reached at 10 nM patupilone. Similar results were obtained with pyruvate, which

protected cells from patupilone as efficiently as tiron. In sharp contrast, addition of tiron or sodium pyruvate at 24 hr of treatment did not modify patupilone activity (Figure 7B-C), indicating that late generation of ROS was not responsible for the drug anti-tumor effects. Altogether, our data show that neuroblastoma cell death induced by patupilone was mediated by the early generation of $O_2^{\circ -}$ and the subsequent formation of H_2O_2 from mitochondria.

Bim early translocates to mitochondria during patupilone-induced apoptosis.

Bim is a pro-apoptotic protein of the Bcl-2 family as well as a cytoskeleton resident protein (Puthalakath et al., 1999; Butt et al., 2006). It thus represents a candidate of choice to be translocated towards mitochondria during patupilone-induced apoptosis. While Bim expression levels did not significantly change in whole cells (Figure 8A), it was modified in the mitochondrial compartment (Figure 8B). Indeed, Bim amount considerably increased (2.4 ± 1.0 fold) in mitochondria isolated from cells treated for only 6 hr with patupilone, as compared with those extracted from control SK-N-SH cells (DMSO-treated) at the same time point. Bim translocation was amplified at 12 hr of treatment (3.3 ± 0.7 fold), until a maximum achieved at 24 hr of treatment (4.7 ± 0.7 fold increased) and maintained at 30 hr. In parallel, we did not detect any modification in Bak or Bcl-2 expression, and Bcl-2 hyperphosphorylation was only observed for patupilone concentrations that induced mitotic block (data not shown). Thus, regarding Bcl-2 family proteins, Bim accumulation to mitochondria was a specific event early induced by patupilone.

In contrast to Bim, p53 expression was increased by patupilone from 12 hr (6.7 ± 0.5 times) in whole SK-N-SH cells (Figure 8C). Since p53 is also a microtubule-transported protein, we evaluated whether it could be displaced to mitochondria during patupilone-induced apoptosis. We observed that the mitochondria-localized p53 increased during treatment (12.3 ± 1.5 times at 30 hr), in contrast with p21 that was completely absent from the

mitochondrial fractions (Figure 8D). However, as accumulation of p53 in mitochondria only started at 12 hr, it may amplify mitochondrial permeabilization subsequently to Bim translocation rather than initiate it.

Reactive oxygen species trigger Bim relocalization and changes in mitochondrial membranes.

Since Bim relocalization to mitochondria occurred early in the apoptotic signaling cascade induced by patupilone, we investigated the role of ROS generation in this process. Of interest, Bim amount was decreased by 2.3 ± 0.2 and 2.9 ± 0.4 times ($p < 0.05$) in mitochondria isolated from SK-N-SH cells treated with patupilone in presence of tiron or sodium pyruvate respectively, as compared with patupilone alone (Figure 9A). Tiron and sodium pyruvate specifically prevented Bim relocalization since no change in Bim expression level was detected in whole cells in the same conditions (data not shown).

Moreover, by inhibiting ROS generation from mitochondria, rotenone also inhibited patupilone-induced Bim translocation (Figure 9B). The specificity of ROS-governed Bim relocalization was shown by the fact that neither Bcl-2 nor Bax mitochondrial levels were modified during treatment. In parallel, cytochrome c release from mitochondria was strongly reduced when patupilone was combined to rotenone (Figure 9B). By electron microscopy, we lastly showed that the “striped” phenotype of mitochondria induced by patupilone (Figure 4) was prevented by tiron (Figure 9C). Altogether, these data indicate that patupilone-mediated production of ROS from mitochondria was responsible for Bim translocation, changes in mitochondrial membrane integrity and the subsequent neuroblastoma cell death.

DISCUSSION

The role of ROS in apoptotic signalling is the subject of growing number of studies in cancer cells (Ryter et al., 2007). Increase in ROS production from mitochondria by taxanes is now well established but ROS contribution to their cytotoxicity is still controversial (Varbiro et al., 2001; André et al., 2002; Park et al., 2004; Fawcett et al., 2005; Patenaude et al., 2007). Moreover, recent reports showed that paclitaxel anticancer activity may also be related to the generation of intracellular and extracellular ROS from the membrane-associated NADPH oxidase (Alexandre et al., 2006; Alexandre et al., 2007). By using anti-oxidants and $\rho^{(-)}$ cells, our current study shows that accumulation of mitochondria-derived $O_2^{\cdot -}$ and H_2O_2 is a causal effect of apoptosis induction by patupilone. Furthermore, we determined for the first time that early produced mitochondrial ROS induced Bim relocalization to mitochondria following MTA treatment.

The involvement of mitochondrial ROS in the apoptotic program leads to the question of the events responsible for the increased ROS generation. We previously showed that patupilone directly modified mitochondrial membrane permeability, suggesting that mitochondria may be the target of choice for patupilone to induce apoptosis through ROS production (Khawaja et al., 2006). Several lines of evidence, mainly obtained during ceramide-induced apoptosis, indicate that ROS accumulation can be due to an impairment of the mitochondrial respiratory chain (Fleury et al., 2002). Depletion of mitochondrial respiratory chain components in $\rho^{(-)}$ neuroblastoma cells abrogated the increase of ROS levels by patupilone, indicating that patupilone induced modulation of ROS production may also originate from the dysfunction of the mitochondrial respiratory chain. In agreement with this hypothesis, we previously showed that paclitaxel disturbed the mitochondrial respiration rate in neuroblastoma cells (André et al., 2002). It should however be noticed that patupilone IC_{50} was equally as active in increasing ROS levels as 10 times IC_{50} of paclitaxel (*i.e.* 1 μ M,)

(André et al., 2002). In addition, we previously showed that patupilone was more efficient than paclitaxel to induce changes in membrane permeability of isolated mitochondria (Khawaja et al., 2006). Altogether, these results may explain a part of the superior activity of patupilone in tumor cells as compared with paclitaxel that is, until now, the clinical reference among microtubule-stabilizing agents. Elsewhere, since functions of mitochondria are tightly regulated by their interactions with the microtubule cytoskeleton (Anesti and Scorrano, 2006), patupilone may influence mitochondrial movements, shape and bioenergetics by modifying microtubule dynamics. Thus, patupilone-mediated ROS production by mitochondria may be related to its ability to strongly stabilize interphasic microtubules during the first 6 hours of treatment (Khawaja et al., 2006). Future investigations will determine whether microtubule directed activity of patupilone is responsible for ROS generation and mitochondrial network disruption.

The molecular link between mitochondrial ROS and MTA activity remains to be established. Here, we showed that the early increase in mitochondrial ROS by patupilone preceded mitochondrial membrane alterations and cytochrome c release. Product of $O_2^{\cdot-}$, H_2O_2 displays the ability to directly affect cellular membranes, including mitochondria themselves by modifying structure and function of lipids (Petrosillo et al., 2003; Fruehauf and Meyskens, 2007). Interestingly, the lipid peroxidation scavenger trolox did not decrease patupilone activity (personal data), suggesting that mediator(s) might be activated by mitochondrial ROS to trigger, in turn, the loss of mitochondrial membrane integrity.

Mitochondrial membrane permeabilization most generally occurs in response to pro-apoptotic members of the Bcl-2 family. In contrast to paclitaxel (Tan et al., 2005), patupilone did not increase Bim expression levels to induce apoptosis. While different models of BH3-only protein interaction with Bax-like and/or Bcl-2-like proteins are currently discussed, it is

assumed that Bim-mediated apoptosis requires mitochondrial targeting (Le Bras et al., 2006). However, except a recent study with the microtubule-depolymerizing agent combretastatin-A4 (Cenciarelli et al., 2008), Bim intracellular distribution has not been evaluated during treatment with MTAs. Our work demonstrates that patupilone early triggered Bim accumulation to mitochondria, which turns the ratio of mitochondria-localized Bcl-2 family proteins in favour of apoptosis. Furthermore, we showed for the first time that Bim accumulation to mitochondria depends on $O_2^{\circ-}$ and H_2O_2 production by mitochondria themselves. More precisely, we determined that ROS generated in the first 6 hours during patupilone-mediated apoptosis were responsible for Bim relocalization. Although H_2O_2 is a relatively weak oxidant, it has emerged as an important signaling molecule mainly based on its capacity to easily diffuse to cellular targets. Since the microtubule network provides the rails for mitochondria trafficking, H_2O_2 may directly affect Bim interaction with microtubules, leading to its translocation to neighboring mitochondria. Elsewhere, Bim activation may also result from its specific phosphorylation by JNK, as described during treatment with a plant toxin (persin) which also acts as a microtubule-stabilizing agent (Butt et al., 2006). In support of this hypothesis, JNK has recently been shown to be activated by ROS during apoptosis (Feng et al., 2007). However, we did not measure an increase in active JNK, and patupilone cytotoxicity was not changed by the specific inhibition of JNK (personal data). These data strongly suggest that JNK is not the kinase responsible for Bim activation and translocation to mitochondria during patupilone-induced apoptosis. Future investigations will determine whether other kinases, such as p38MAPK, could be activated by ROS and phosphorylate Bim. Whatever the event responsible for its release, Bim appears to be a molecular mediator to bridge the effects of patupilone on both microtubules and mitochondria.

MOL #48405

New insights into apoptotic pathways are urgently needed to promote development of rationally targeted cancer therapeutics. The role of ROS in cancer cell response to drugs is emerging as an important area of exploration. Altogether, our data identified ROS generation from mitochondria as a central event mediating apoptosis induced by patupilone. They also suggest a key communication between microtubules, which govern intracellular transport, and mitochondria, compartment which plays simultaneously the role of activator and integrator of apoptotic signals.

REFERENCES

- Adams JM and Cory S (2007) The Bcl-2 apoptotic switch in cancer development and therapy. *Oncogene* **26**:1324-1337.
- Alexandre J, Batteux F, Nicco C, Chéreau C, Laurent A, Guillevin L, Weill B and Goldwasser F (2006) Accumulation of hydrogen peroxide is an early and crucial step for paclitaxel-induced cancer cell death both in vitro and in vivo. *Int J Cancer* **119**:41-48.
- Alexandre J, Hu Y, Lu W, Pelicano H and Huang P (2007) Novel action of paclitaxel against cancer cells: bystander effect mediated by reactive oxygen species. *Cancer Res.***67**:3512-3517.
- Altmann KH, Pfeiffer B, Arseniyadis S, Pratt BA and Nicolaou KC (2007) The Chemistry and Biology of Epothilones-The Wheel Keeps Turning. *Chem Med Chem* **2**:396-423.
- André N, Carré M, Brasseur G, Pourroy B, Kovacic H, Briand C and Braguer D (2002) Paclitaxel targets mitochondria upstream of caspase activation in intact human neuroblastoma cells. *FEBS Lett* **532**:256-260.
- André N, Braguer D, Brasseur G, Gonçalves A, Lemesle-Meunier D, Guise S, Jordan MA and Briand C (2000) Paclitaxel Induces Release of Cytochrome *c* from Mitochondria Isolated from Human Neuroblastoma Cells. *Cancer Res* **60**:5349-5353.
- Anesti V and Scorrano L (2006) The relationship between mitochondrial shape and function and the cytoskeleton. *Biochim Biophys Acta* **1757**:692-699.
- Archer SL, Gomberg-Maitland M, Maitland ML, Rich S, Garcia JG and Weir EK (2008) Mitochondrial metabolism, redox signaling, and fusion: a mitochondria-ROS-HIF-1 α -Kv1.5 O₂-sensing pathway at the intersection of pulmonary hypertension and cancer. *Am J Physiol Heart Circ Physiol.* **294**:570-578.

- Bollag DM, McQueney PA, Zhu J, Hensens O, Koupal L, Liesch J, Goetz M, Lazarides E and Woods CM (1995) Epothilones, a new class of microtubule-stabilizing agents with a taxol-like mechanism of action. *Cancer Res* **55**:2325-2333.
- Butt AJ, Roberts CG, Seawright AA, Oelrichs PB, Macleod JK, Liaw TY, Kavallaris M, Somers-Edgar TJ, Lehrbach GM, Watts CK and Sutherland RL (2006) A novel plant toxin, persin, with in vivo activity in the mammary gland, induces Bim-dependent apoptosis in human breast cancer cells. *Mol Cancer Ther* **5**:2300-2309.
- Cenciarelli C, Tanzarella C, Vitale I, Pisano C, Crateri P, Meschini S, Arancia G and Antoccia A (2008) The tubulin-depolymerising agent combretastatin-4 induces ectopic aster assembly and mitotic catastrophe in lung cancer cells H460. *Apoptosis*. **13**:659-669.
- Estève M.A, Carré M, Bourgarel-Rey V, Kruczynski A, Raspaglio G, Ferlini C and Braguer D (2006) Bcl-2 down-regulation and tubulin subtype composition are involved in resistance of ovarian cancer cells to vinflunine. *Mol Cancer Ther* **5**:2824-2833.
- Estève M.A, Carré M and Braguer D (2007) Microtubules in apoptosis induction: are they necessary? *Curr Cancer Drug Targets* **7**:713-729.
- Fawcett H, Mader JS, Robichaud M, Giacomantonio C and Hoskin DW (2005) Contribution of reactive oxygen species and caspase-3 to apoptosis and attenuated ICAM-1 expression by paclitaxel-treated MDA-MB-435 breast carcinoma cells. *Int J Oncol*. **27**:1717-1726.
- Feng R, Ni HM, Wang SY, Tourkova IL, Shurin MR, Harada H AND Yin XM (2007) Cyanidin-3-rutinoside, a natural polyphenol antioxidant, selectively kills leukemic cells by induction of oxidative stress. *J Biol Chem* **282**:13468-13476.
- Ferlini C, Raspaglio G, Mozzetti S, Distefano M, Filippetti F, Martinelli E, Ferrandina G, Gallo D, Ranelletti FO and Scambia G (2003) Bcl-2 down-regulation is a novel mechanism of paclitaxel resistance. *Mol Pharmacol* **64**:51-58.

- Fleury C, Mignotte B and Vayssière JL (2002) Mitochondrial reactive oxygen species in cell death signaling. *Biochimie* **84**:131-141.
- Fruehauf JP and Meyskens FL Jr (2007) Reactive oxygen species: a breath of life or death? *Clin Cancer Res* **13**:789-794.
- Honoré S, Kovacic H, Pichard V, Briand C and Rognoni JB (2003) $\alpha 2\beta 1$ -integrin signaling by itself controls G1/S transition in a human adenocarcinoma cell line (Caco-2): implication of NADPH oxidase-dependent production of ROS. *Experimental Cell Research* **285**:59-71.
- Jordan MA and Kamath K (2007) How do microtubule-targeted drugs work? An overview. *Curr Cancer Drug Targets* **7**:730-742.
- Le Bras M, Rouy I and Brenner C (2007) The modulation of inter-organelle cross-talk to control apoptosis. *Med Chem* **2**:1-12.
- Lee FY, Smykla R, Johnston K, Menard K, McGlinchey K, Peterson RW, Wiebesiek A, Vite G, Fairchild CR and Kramer R (2008) Preclinical efficacy spectrum and pharmacokinetics of ixabepilone. *Cancer Chemother Pharmacol* "in press"
- Li R, Moudgil T, Ross HJ and hu HM (2005) Apoptosis of non-small-cell lung cancer cell lines after paclitaxel treatment involves the BH3-only proapoptotic protein Bim. *Cell Death Differ* **12**:292-303.
- Li Z, Zhang J, Liu Z, Woo CW and Thiele CJ (2007) Downregulation of Bim by brain-derived neurotrophic factor activation of TrkB protects neuroblastoma cells from paclitaxel but not etoposide or cisplatin-induced cell death. *Cell Death Differ* **14**:318-326.
- Morazzani M, de Carvalho DD, Kovacic H, Smida-Rezgui S, Briand C and Penel C (2004) Monolayer versus aggregate balance in survival process for EGF-induced apoptosis in A431 carcinoma cells: Implication of ROS-P38 MAPK-integrin $\alpha 2\beta 1$ pathway. *Int J Cancer* **110**:788-799.

- Nettles JH, Li H, Cornett B, Krahn JM and Snyder JP (2004) Downing KH. The binding mode of epothilone A on alpha,beta-tubulin by electron crystallography. *Science* **5**:866-869.
- Newmeyer DD and Ferguson-Miller S (2003) Mitochondria: releasing power for life and unleashing the machineries of death. *Cell* **112**:481-490.
- Nicolaou KC, Winssinger N, Pastor J, Ninkovic S, Sarabia F, He Y, Vourloumis D, Yang Z, Li T, Giannakakou P and Hamel E (1997) Synthesis of epothilones A and B in solid and solution phase. *Nature* **387**:268-272
- Orr GA, Verdier-Pinard P, McDaid H and Horwitz SB (2003) Mechanisms of Taxol resistance related to microtubules. *Oncogene* **22**:7280-7295.
- Park SJ, Wu CH, Gordon JD, Zhong X, Emami A and Safa AR (2004) Taxol induces caspase-10-dependent apoptosis. *J Biol Chem* **279**:51057-51067.
- Pasquier E, Honoré S and Braguer D (2006) Microtubule-targeting agents in angiogenesis: where do we stand? *Drug Resist Updat* **9**:74-86.
- Patenaude A, Deschesnes RG, Rousseau JL, Petitclerc E, Lacroix J, Côté MF and C-Gaudreault R (2007) New soft alkylating agents with enhanced cytotoxicity against cancer cells resistant to chemotherapeutics and hypoxia. *Cancer Res* **67**:2306-2316.
- Petrosillo G, Ruggiero FM and Paradies G (2003) Role of reactive oxygen species and cardiolipin in the release of cytochrome c from mitochondria. *FASEB J* **17**:2202-2208.
- Pourroy B, Carré M, Honoré S, Bourgarel-Rey V, Kruczynski A, Briand C and Braguer D (2004) Low Concentrations of Vinflunine Induce Apoptosis in Human SK-N-SH neuroblastoma Cells through a Postmitotic G₁ Arrest and a Mitochondrial Pathway. *Mol Pharmacol* **66**:580-591.

- Putcha GV, Moulder KL, Golden JP, Bouillet P, Adams JA, Strasser A and Johnson EM (2001) Induction of BIM, a proapoptotic BH3-only BCL-2 family member, is critical for neuronal apoptosis. *Neuron* **29**:615-628.
- Puthalakath H, Huang DC, O'Reilly LA, King SM and Strasser A (1999) The Proapoptotic Activity of the Bcl-2 Family Member Bim Is Regulated by Interaction with the Dynein Motor Complex. *Molecular Cell* **3**:287-296.
- Ryter SW, Kim HP, Hoetzel A, Park JW, Nakahira K, Wang X and Choi AM (2007) Mechanisms of cell death in oxidative stress. *Antioxid Redox Signal* **9**:49-89.
- Sève P, Reiman T, Lai R, Hanson J, Santos C, Johnson L, Dabbagh L, Sawyer M, Dumontet C and Mackey JR (2007) Class III beta-tubulin is a marker of paclitaxel resistance in carcinomas of unknown primary site. *Cancer Chemother Pharmacol* **60**:27-34.
- Tan TT, Degenhardt K, Nelson DA, Beaudoin B, Nieves-Neira W, Bouillet P, Villunger A, Adams JM and White E (2005) Key roles of BIM-driven apoptosis in epithelial tumors and rational chemotherapy. *Cancer Cell* **7**:227-238.
- Taniguchi T, Takahashi M, Shinohara F, Sato T, Echigo S and Rikiishi H (2005) Involvement of NF-kappaB and mitochondrial pathways in docetaxel-induced apoptosis of human oral squamous cell carcinoma. *Int J Mol Med* **15**:667-673.
- Varbiro G, Veres B, Gallyas F Jr and Sumegi B (2001) Direct effect of Taxol on free radical formation and mitochondrial permeability transition. *Free Radic Biol Med* **31**:548-558.

FOOTNOTES

This work was partly supported by the Cancéropole PACA and INCa (France) and Khawaja NR received a fellowship from the Higher Education Commission (HEC) Islamabad, Pakistan.

Naeem Raza Khawaja, Manon Carre, Bertrand Pourroy, Herve Kovacic and Diane Braguer (2006) High potency of epothilones in neuroblastoma cells may involve mitochondria. Proceedings of 96th annual meeting of American association of Cancer Research (AACR) Washington DC. *Experimental and Molecular Therapeutics 1: Antimicrotubule agents*.

Reprint requests should be sent to: Pr. D. Braguer, INSERM UMR911, Faculté de Pharmacie, 27 Bd Jean Moulin, 13385 Marseille Cedex 05, France.

E-mail: diane.braguer@univmed.fr

FIGURE LEGENDS

Figure 1. Patupilone potently inhibits cell growth of human neuroblastoma SK-N-SH cells.

(A) Concentration-dependent inhibition of cell survival by patupilone (epothilone B) and epothilone A following a 72 hr treatment. (B) Table showing IC values for both epothilones and paclitaxel in SK-N-SH cells. (C) SK-N-SH cells were treated with indicated patupilone concentrations for 6 hr, 24 hr and 72 hr. After short term treatment (6hr or 24 hr) culture medium with drug was replaced by normal culture medium. MTT assay was performed at 72 hr after treatment in either condition (* = $p < 0.05$ versus control). Results represent means \pm SD.

Figure 2. Patupilone induces apoptosis, regardless of multidrug resistance status. (A)

Fluorescence analysis of nuclei fragmentation after a 48-hr treatment of SK-N-SH cells with patupilone IC₇₀ (40 x objective). Results are representative of three independent experiments.

(B) SK-N-SH cell cycle analysis by flow cytometry. The sub-G₁ population is indicated by an arrow and the corresponding percentage is indicated. (C) Sensitivity of SK-N-SH cells to patupilone and paclitaxel at their respective IC₅₀ (2 and 100 nM) in presence or absence of verapamil 10 μ M. Data are expressed as mean \pm SD (* = $p < 0.05$ versus control).

Figure 3. Patupilone induces changes in mitochondrial membrane permeability. (A)

Measurement of the mitochondrial membrane potential collapse by DIOC₆ incorporation in human neuroblastoma SK-N-SH cells. (B) Western blot analysis of cytochrome c contained in mitochondria isolated from SK-N-SH cells treated with Patupilone IC₇₀ (up to 36 hr). (C)

Immunofluorescence analysis of cytochrome c after a 24-hr treatment with patupilone. Arrows show typical cells with released cytochrome c. Blots, pictures and cytograms are representative of at least three independent experiments. Results were expressed as mean \pm

SD, and significant differences were determined as compared with vehicle-treated cells (* = $p < 0.05$).

Figure 4. Patupilone induces changes in mitochondria morphology. Visualization, by transmission electron microscopy, of mitochondria morphology in SK-N-SH cells treated with vehicle (control) or patupilone IC₇₀. Arrows show typical control mitochondria in the left column and both “striped” (6-20 hr) and swelled mitochondria (40 hr) in the right column. Bar length = 2μm.

Figure 5. Patupilone induces ROS production from mitochondria. **(A)** Relative production of superoxide ions in SK-N-SH cells during patupilone treatment. **(B)** Generation of hydrogen peroxide in SK-N-SH cells incubated with patupilone alone, ROS inhibitors/scavengers alone, or their combinations for 2 or 6 hr. Pyr = sodium pyruvate, rot = rotenone, TR = tiron and ALP = allopurinol **(C)** Relative superoxide generation in ρ⁽⁺⁾ SK-N-SH and ρ⁽⁻⁾ SK-N-SH cells under patupilone (IC₇₀) treatment in presence or absence of rotenone. Data shown are mean ± SD (* = p < 0.05 versus control).

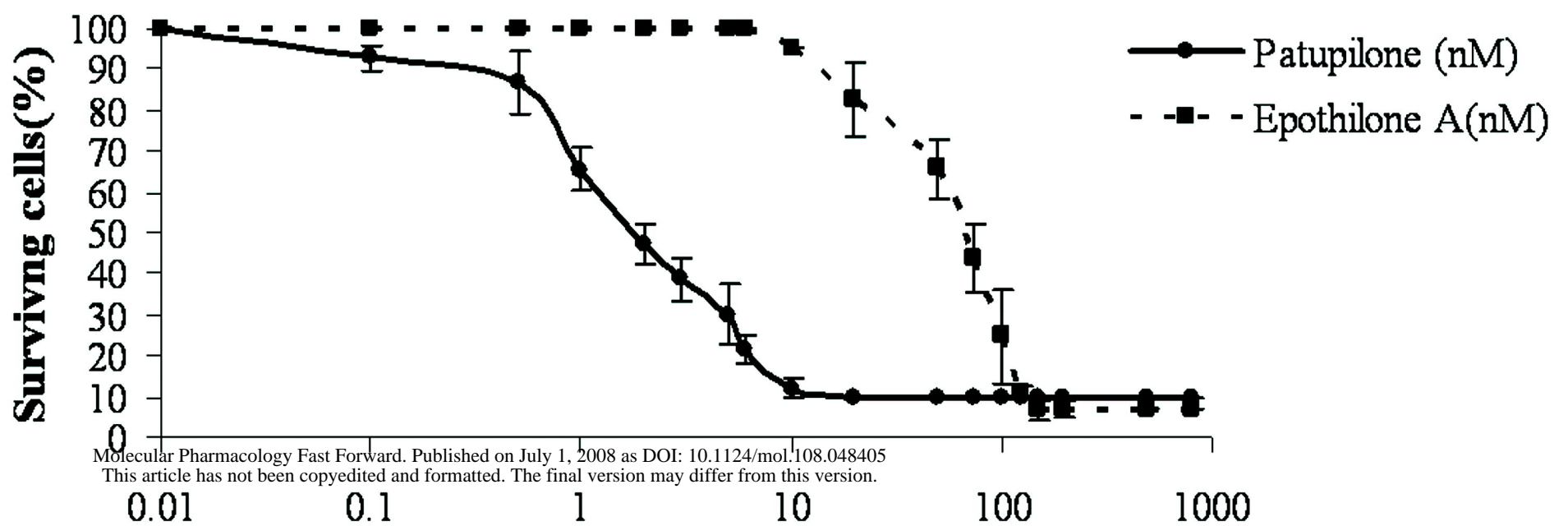
Figure 6. Decreased expression of COX II in ρ⁽⁻⁾ SK-N-SH cells. **(A)** Western blot analysis of COX II, VDAC and other indicated proteins **(B)** in whole cell lysates of ρ⁽⁺⁾SK-N-SH cells and derived ρ⁽⁻⁾SK-N-SH cells. Histogram is outcome of protein quantification by software Image J, and represents mean ± SD (* = p < 0.05 versus control).

Figure 7. Mitochondrial ROS participate in patupilone cytotoxicity. **(A)** Comparison between ρ⁽⁺⁾SK-N-SH and ρ⁽⁻⁾SK-N-SH cells sensitivity to patupilone after a 72 hr-treatment. Concentration-dependent inhibition of SK-N-SH cell survival by patupilone alone after 72 hr treatment or combined with **(B)** tiron (TR) and **(C)** sodium pyruvate (Pyr). ROS scavengers were added at indicated time points, from the beginning (0 hr) and 24 hr, during Patupilone treatment. Results are expressed as mean ± SD.

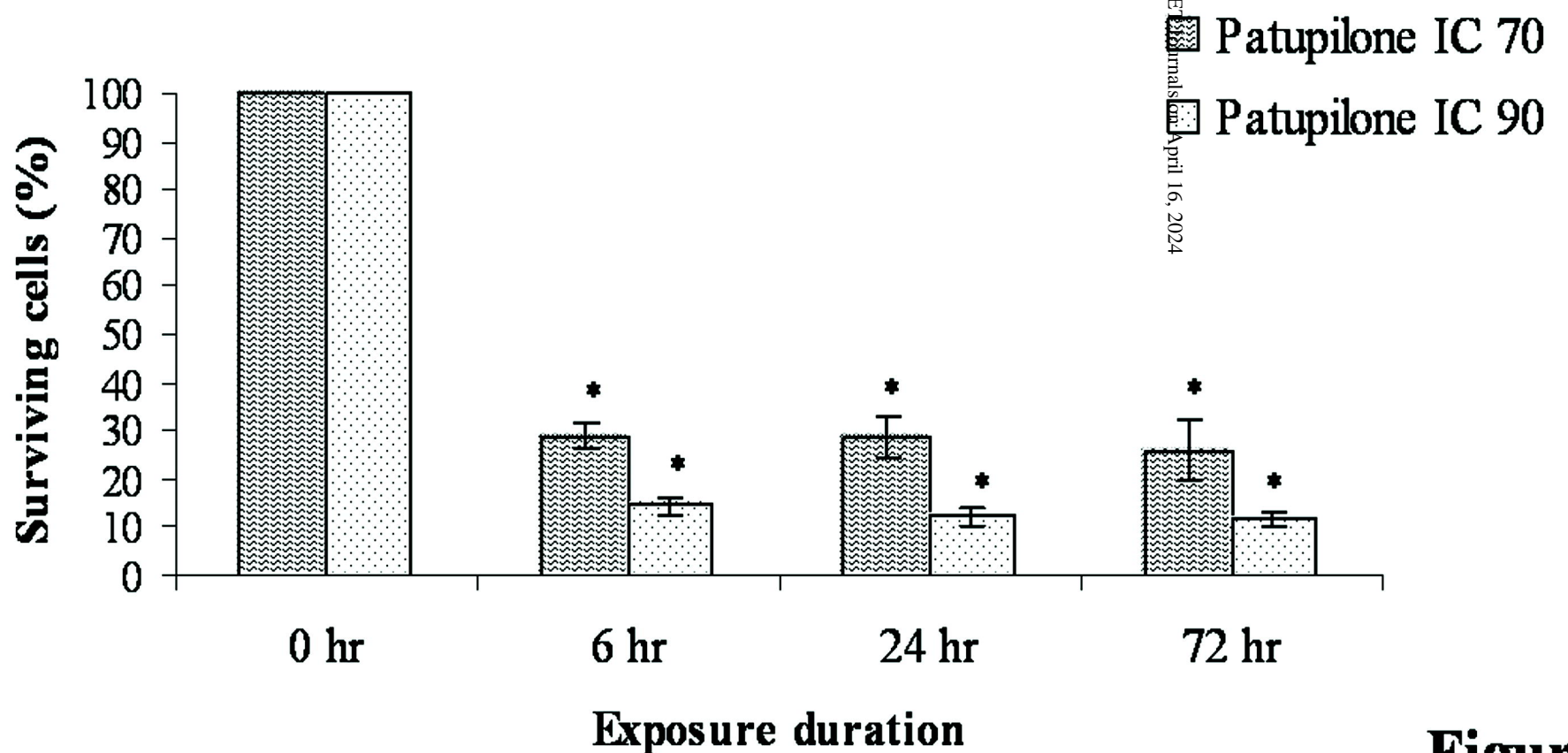
Figure 8. Patupilone induces Bim and p53 accumulation in mitochondria. Relative quantities of **(A)** Bim and **(C)** p53 proteins in whole cells treated with Patupilone IC₇₀. Western blot

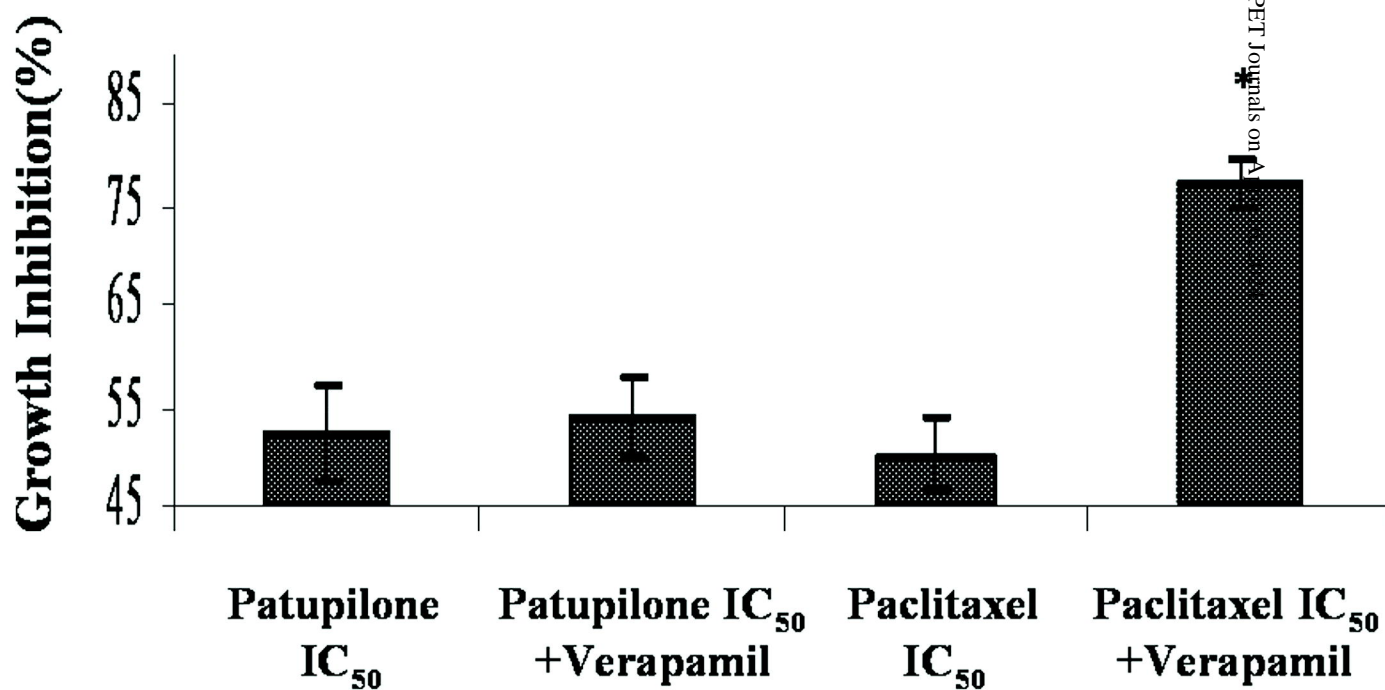
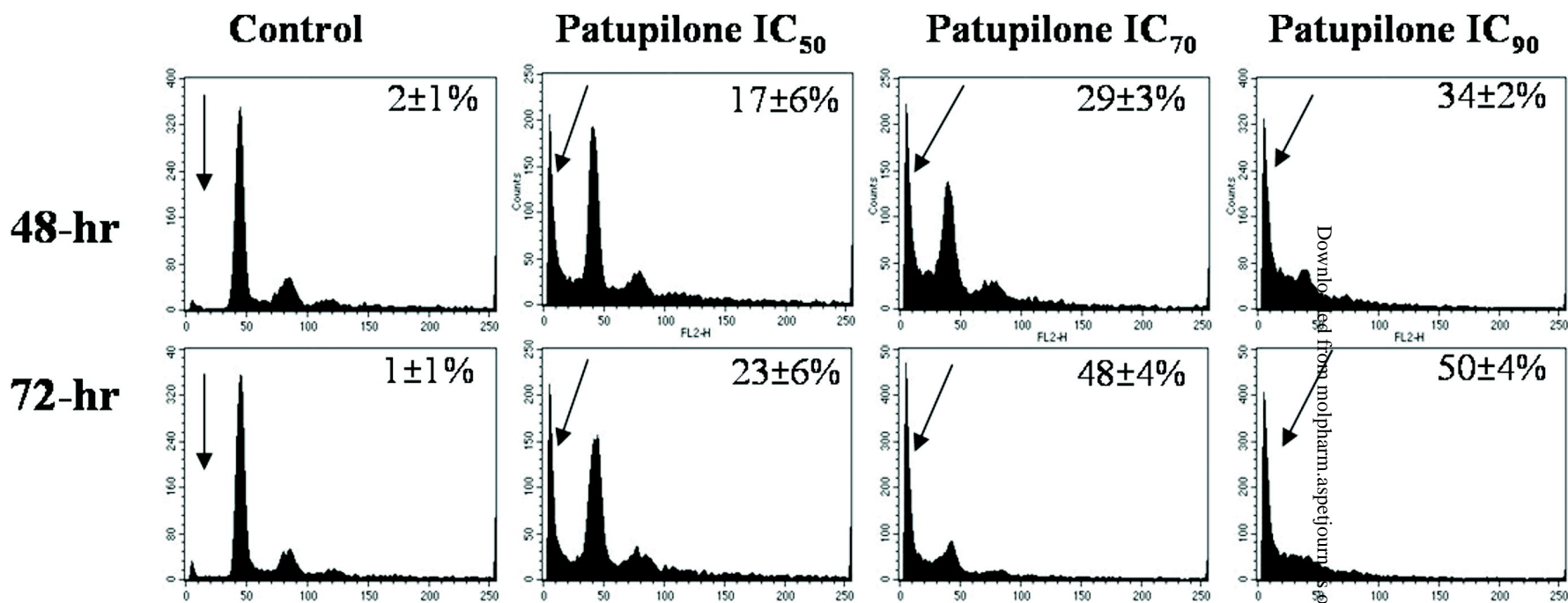
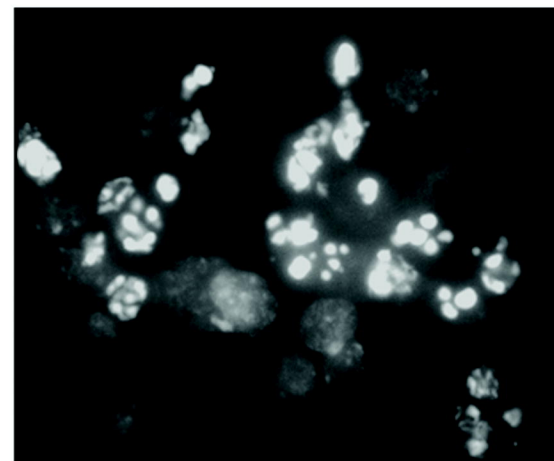
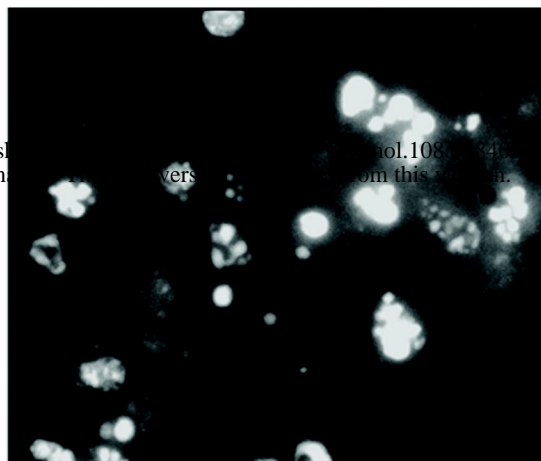
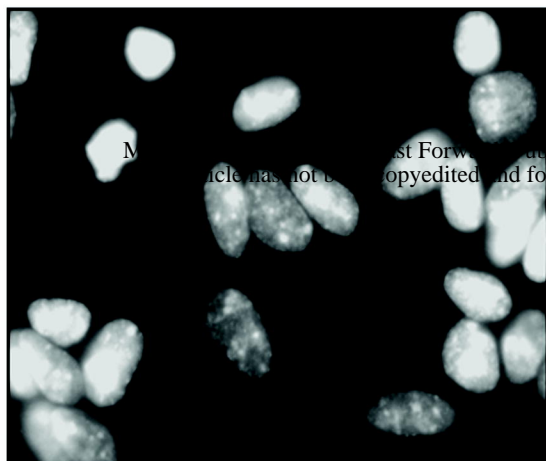
analysis of **(B)** Bim, **(D)** p53 and p21 variations in mitochondrial fractions. Mitochondria were isolated from SK-N-SH cells after treatment with Patupilone IC₇₀ or vehicle (up to 30 hr). Histograms are outcome of respective proteins quantification by software Image J. Results were expressed as mean \pm SD (* = $p < 0.05$ versus control).

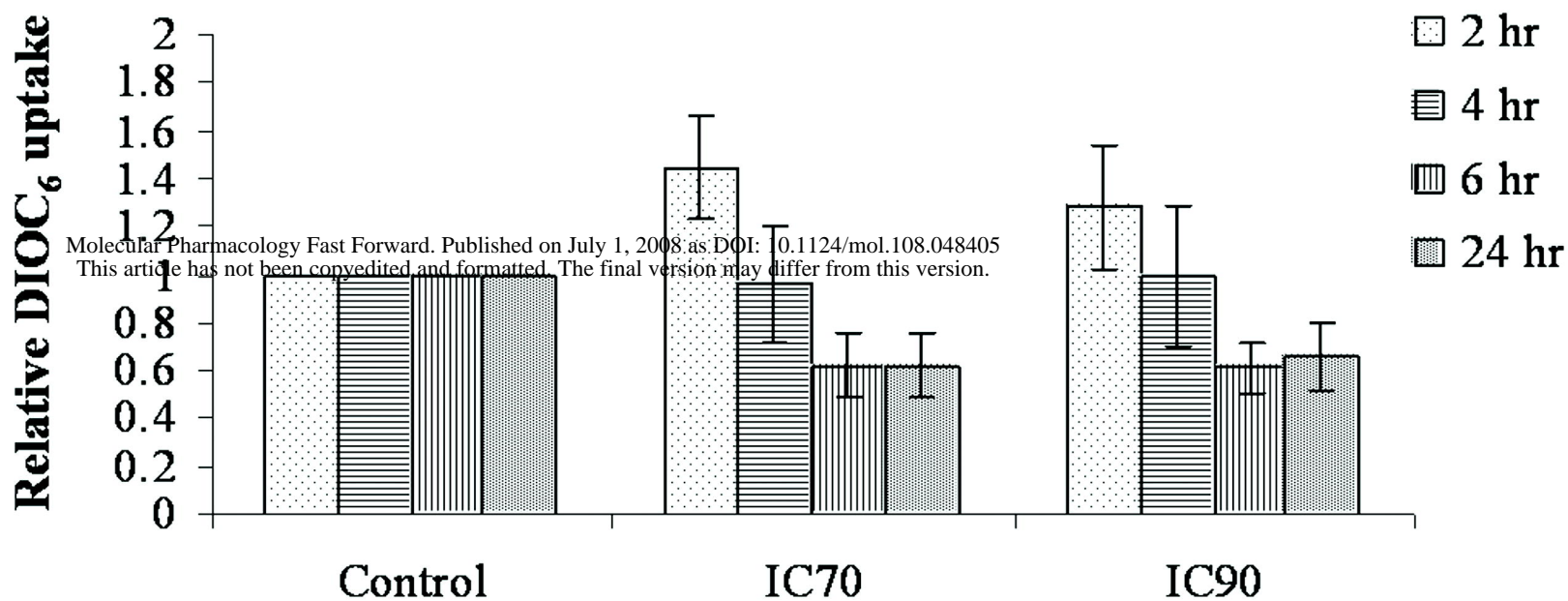
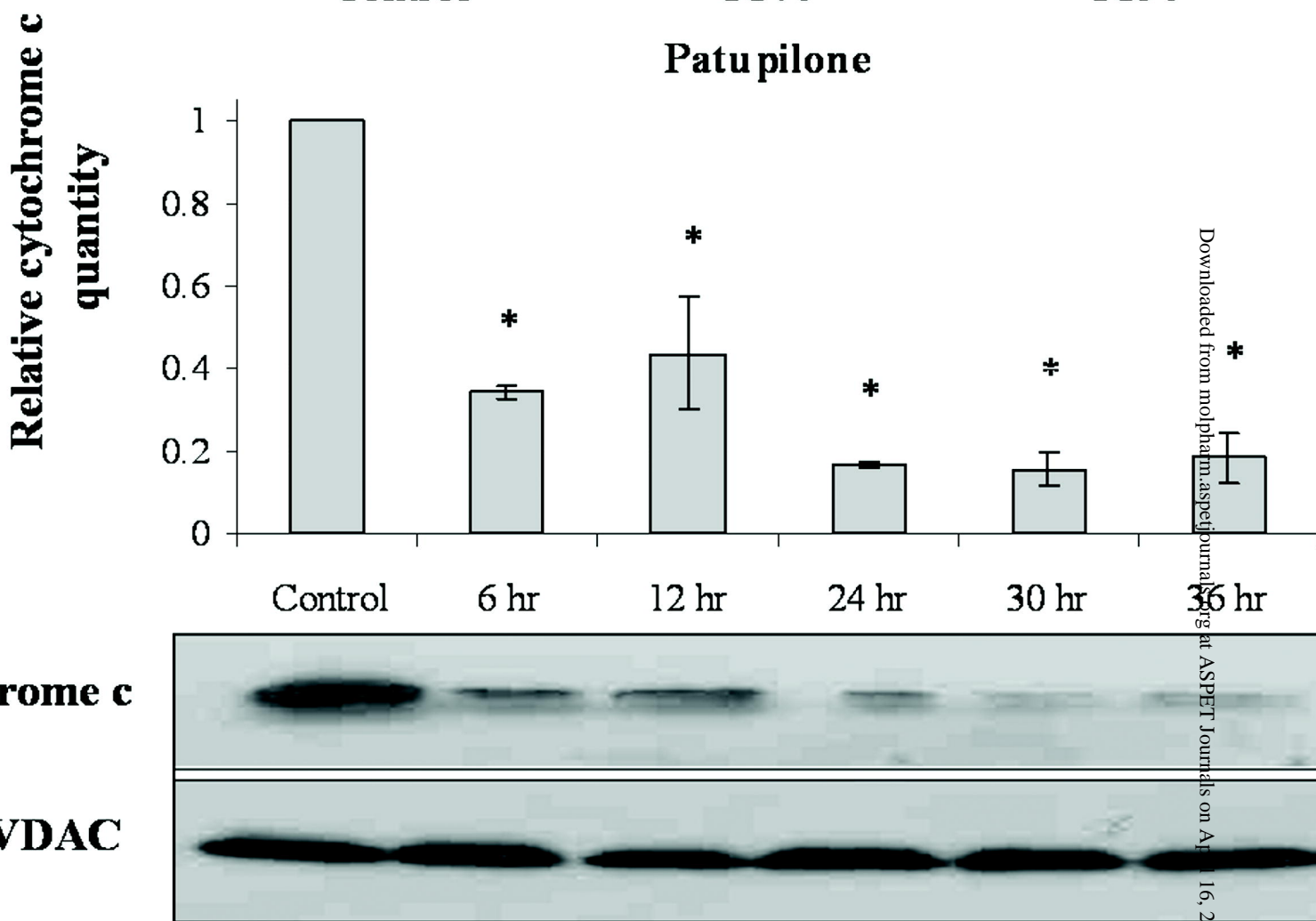
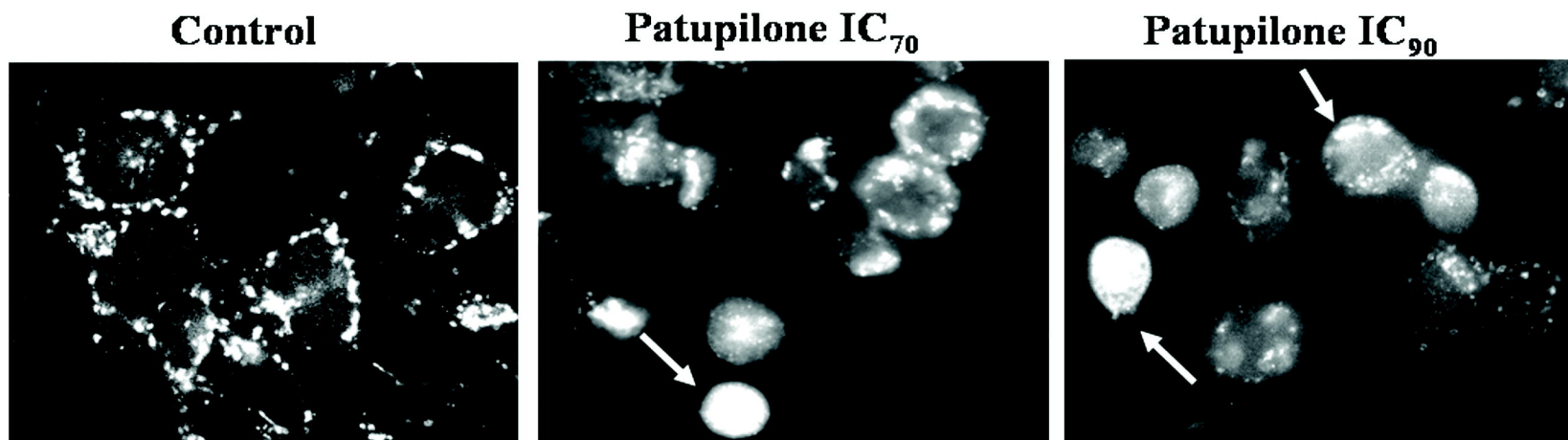
Figure 9. Mitochondrial ROS trigger Bim relocalization to mitochondria and induce mitochondrial membrane changes. **(A)** Western blot analysis of Bim in mitochondrial fractions. SK-N-SH cells were incubated with patupilone IC₇₀ and/or ROS scavengers for 15 hr before isolation of mitochondria. Histogram is outcome of protein quantification by software Image J, and represents mean \pm SD (* = $p < 0.05$ versus control). **(B)** Western blot directed against Bim, cytochrome c, Bcl-2 and Bax in the mitochondrial compartment. Cells were incubated with patupilone IC₇₀ and/or rotenone for 6 hr before isolation of mitochondria. **(C)** Visualisation, by transmission electron microscopy, of mitochondria morphology in SK-N-SH cells treated for 12 hr with tiron alone or combined with patupilone. Arrows show typical normal mitochondria. Bar length = 2 μ m.

A**B**

| IC VALUE | Patupilone (nM) | Epothilone A (nM) | Paclitaxel (nM) |
|------------------|-----------------|-------------------|-----------------|
| IC ₃₀ | 1 | 50 | 50 |
| IC ₅₀ | 2 | 70 | 100 |
| IC ₇₀ | 5 | 90 | 150 |
| IC ₉₀ | 10 | 150 | 200 |

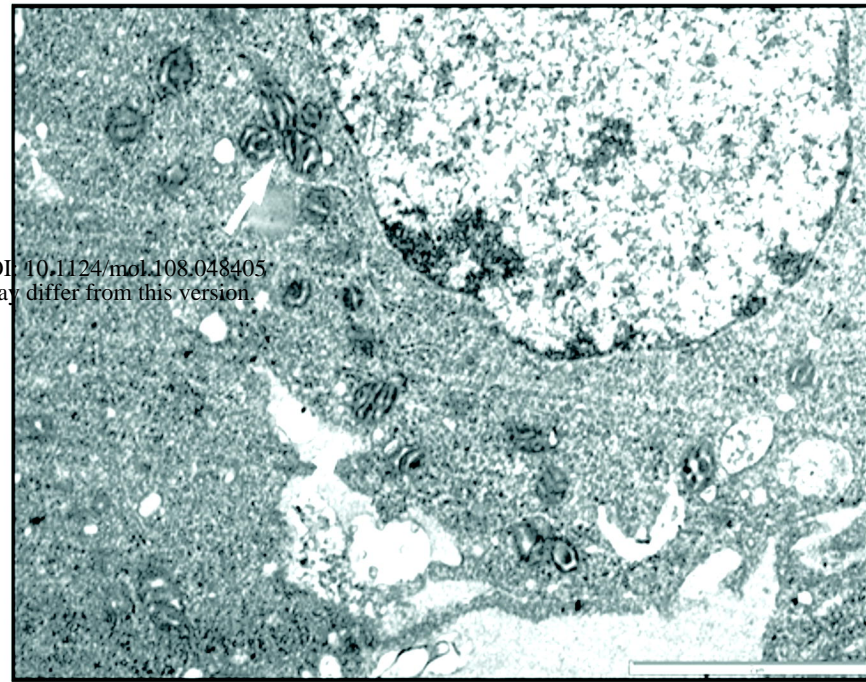
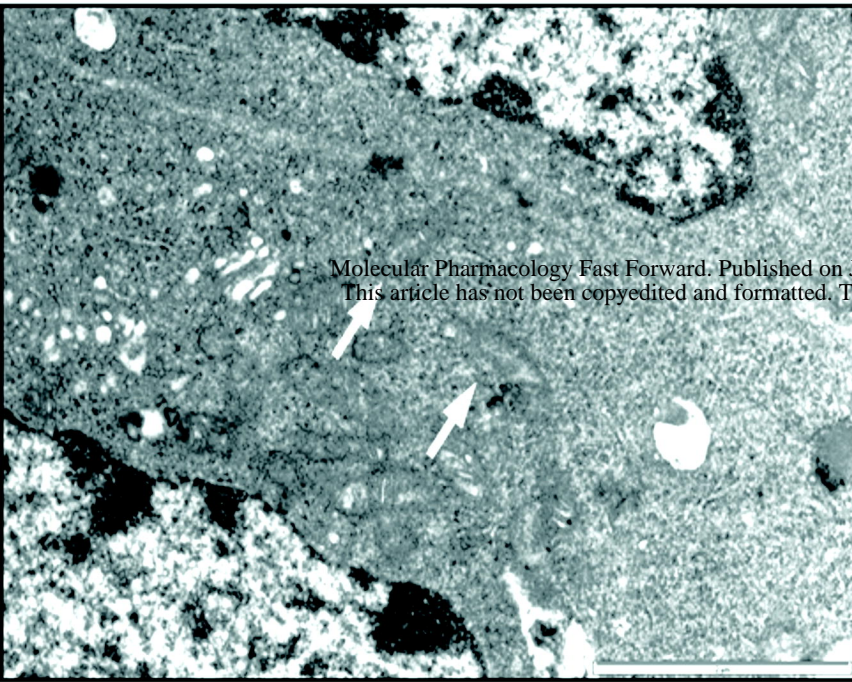
C**Figure 1**

A**Control****Patupilone IC₇₀****Patupilone IC₉₀****Figure 2**

A**B****C****Figure 3**

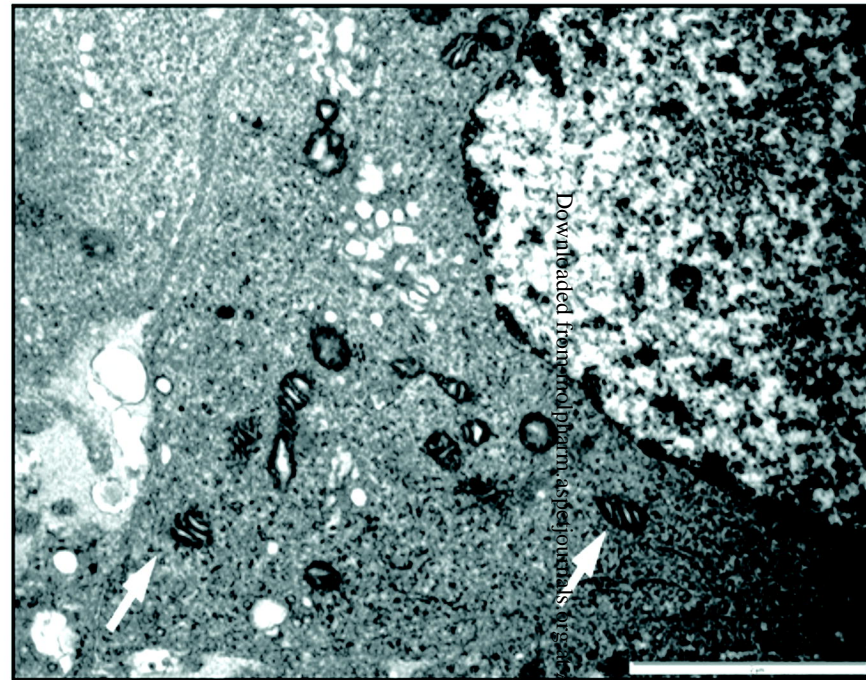
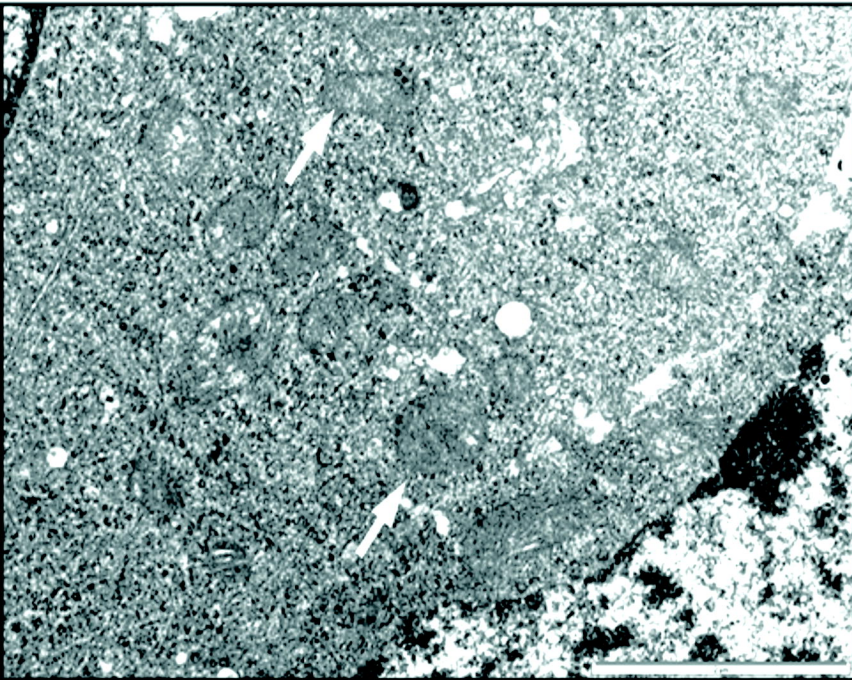
Control

Patupilone IC₇₀

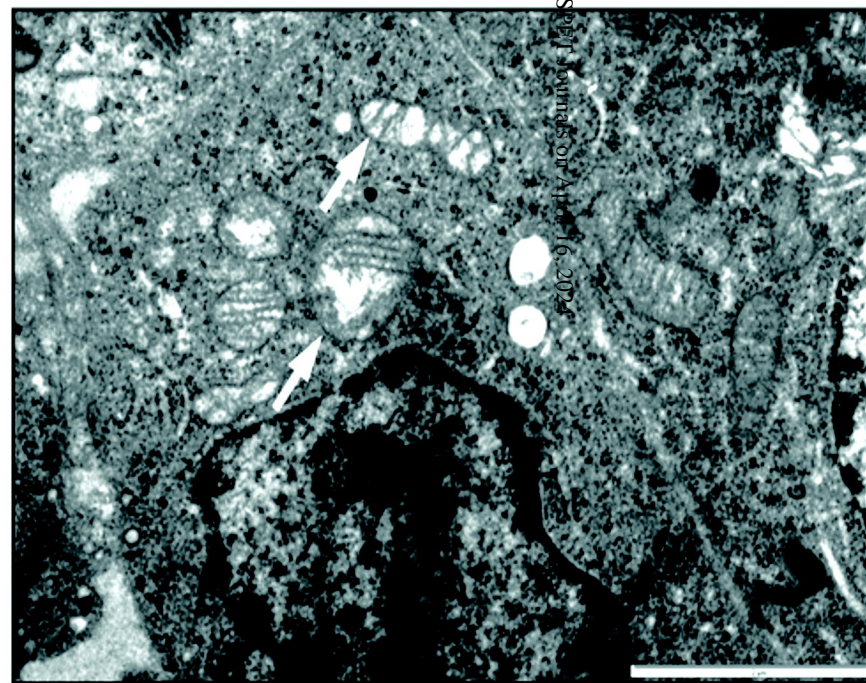
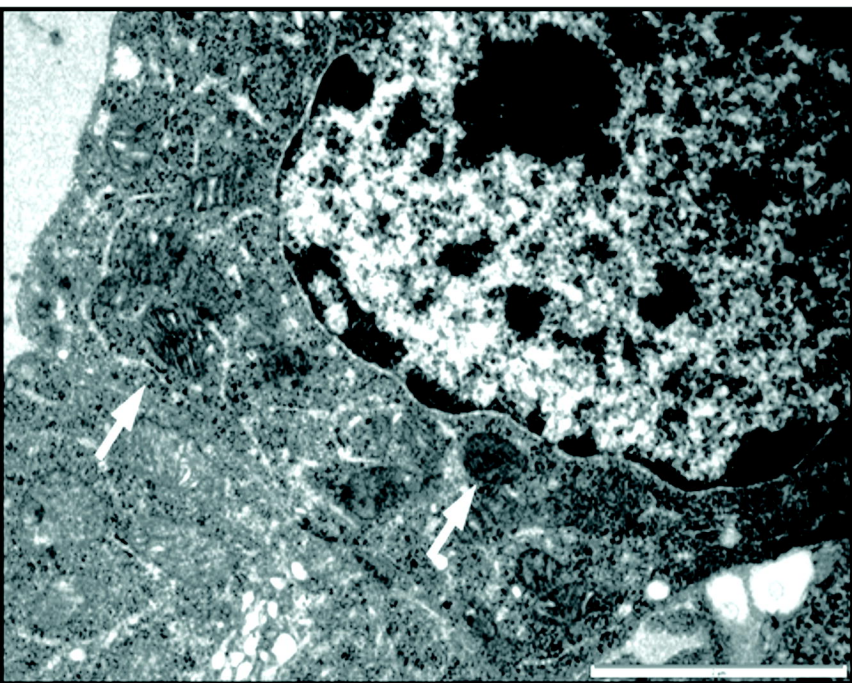


Molecular Pharmacology Fast Forward. Published on July 1, 2008 as DOI 10.1124/mol.108.048405
This article has not been copyedited and formatted. The final version may differ from this version.

6-hr



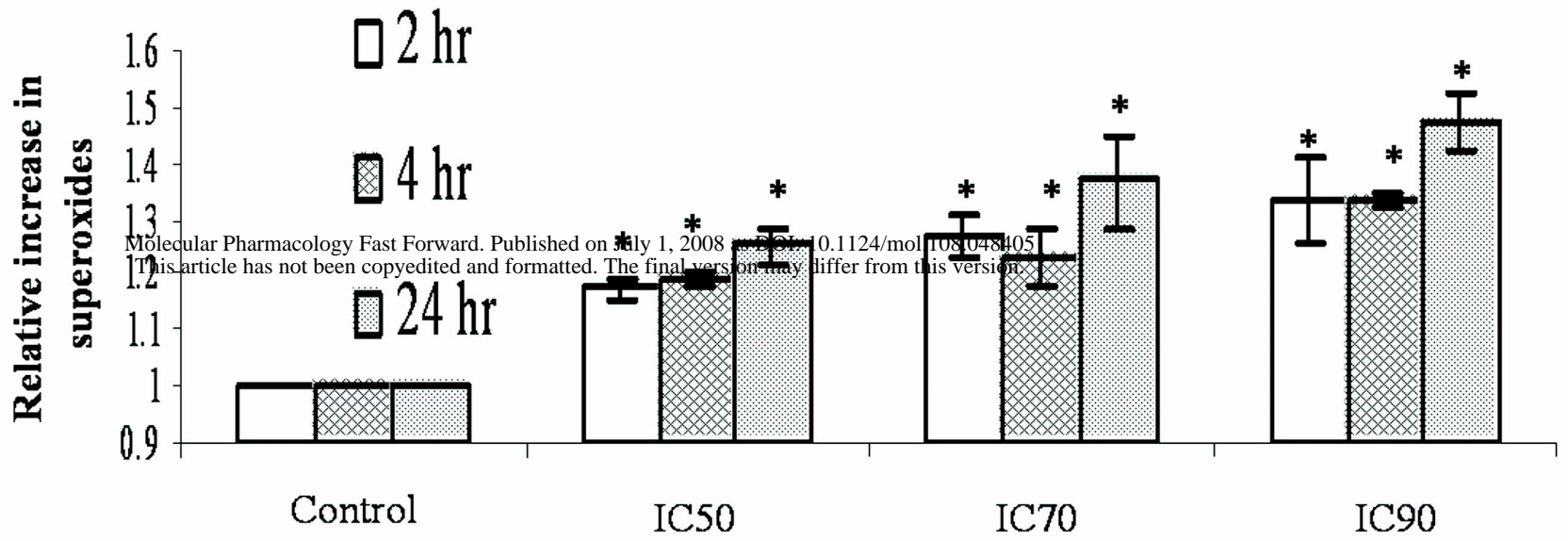
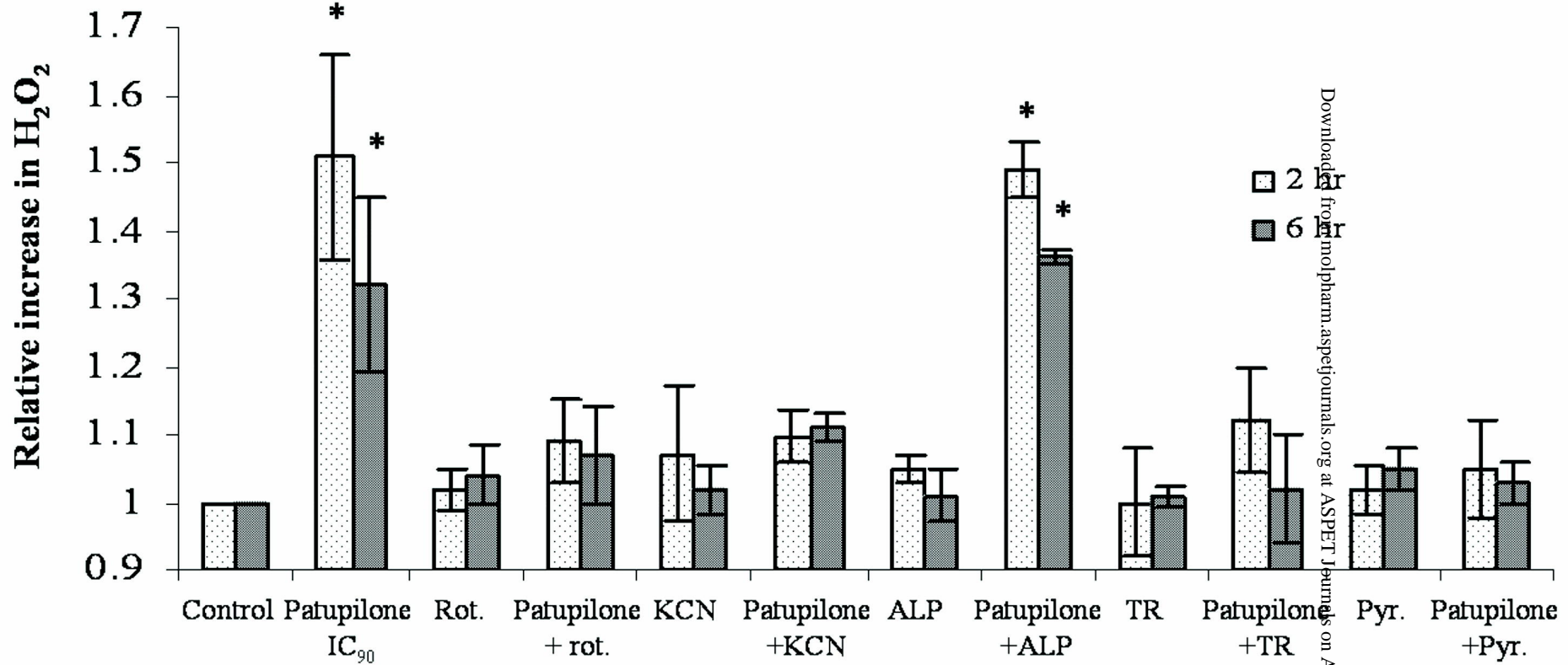
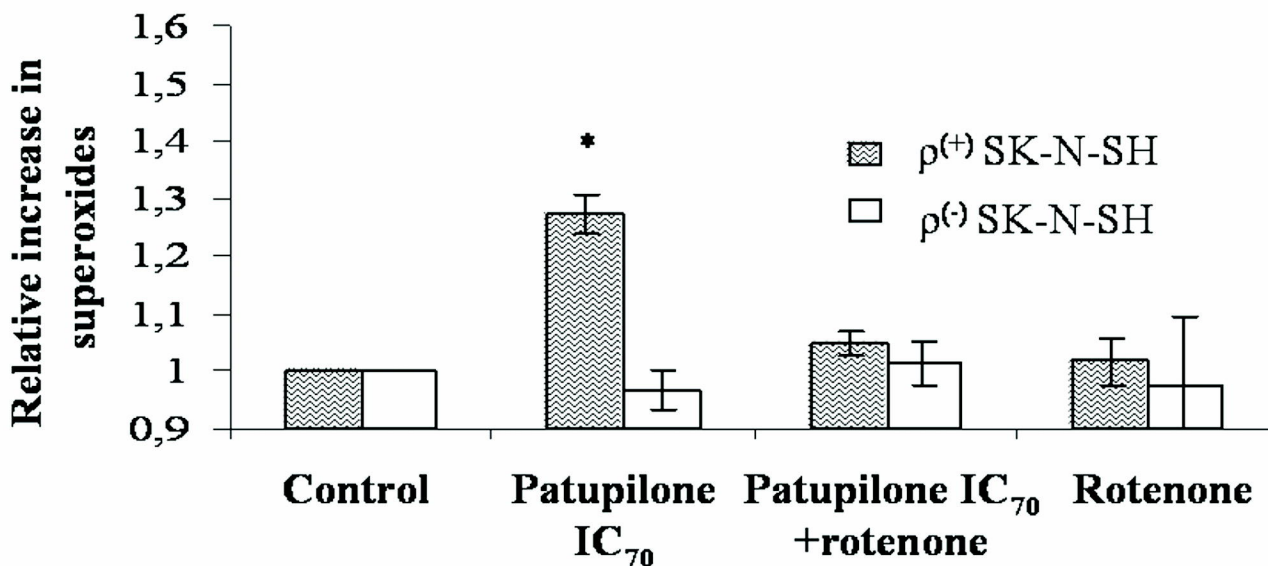
20-hr



40-hr

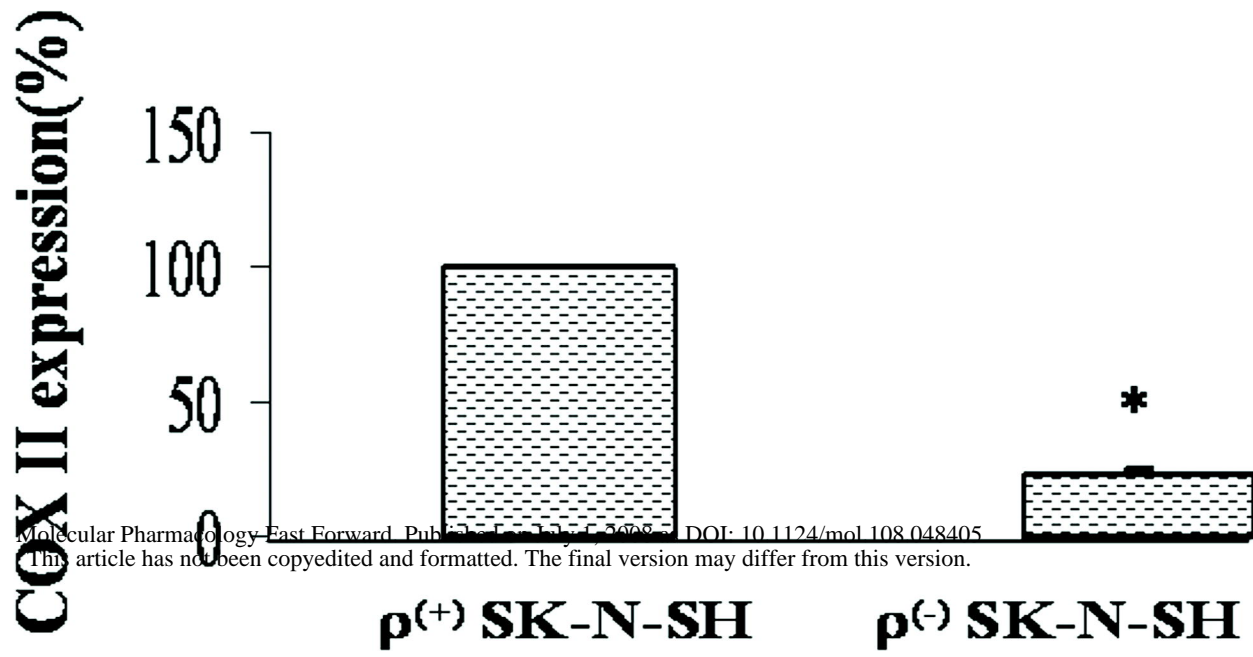
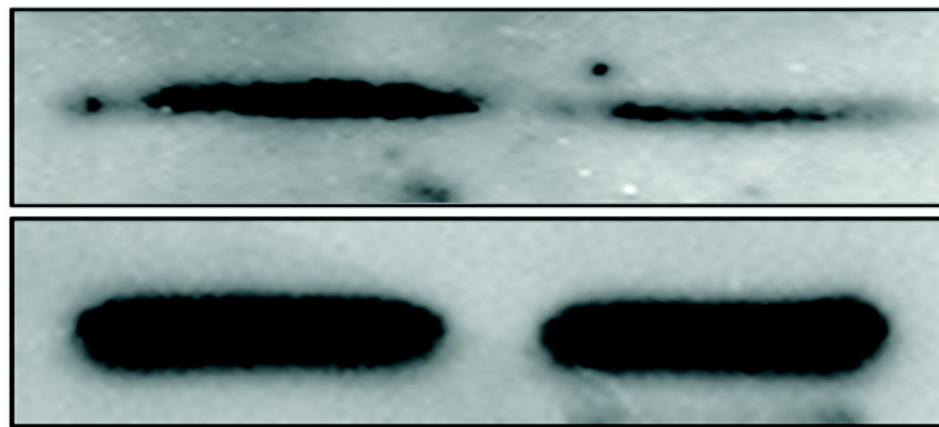
Downloaded from molpharm.asphpubs.org at Seattle University on April 16, 2024

Figure 4

A**B****C**

Downloaded from molpharm.aspetjournals.org at ASPET Journals on April 16, 2024

Figure 5

A**COX II****VDAC****B****p⁽⁺⁾ SK-N-SH** **p⁽⁻⁾ SK-N-SH****Bcl-2****Bim****Bax****Cytochrome c****α-Tubulin**

Downloaded from molpharm.aspetjournals.org at ASHET Journals on April 16, 2024

Figure 6

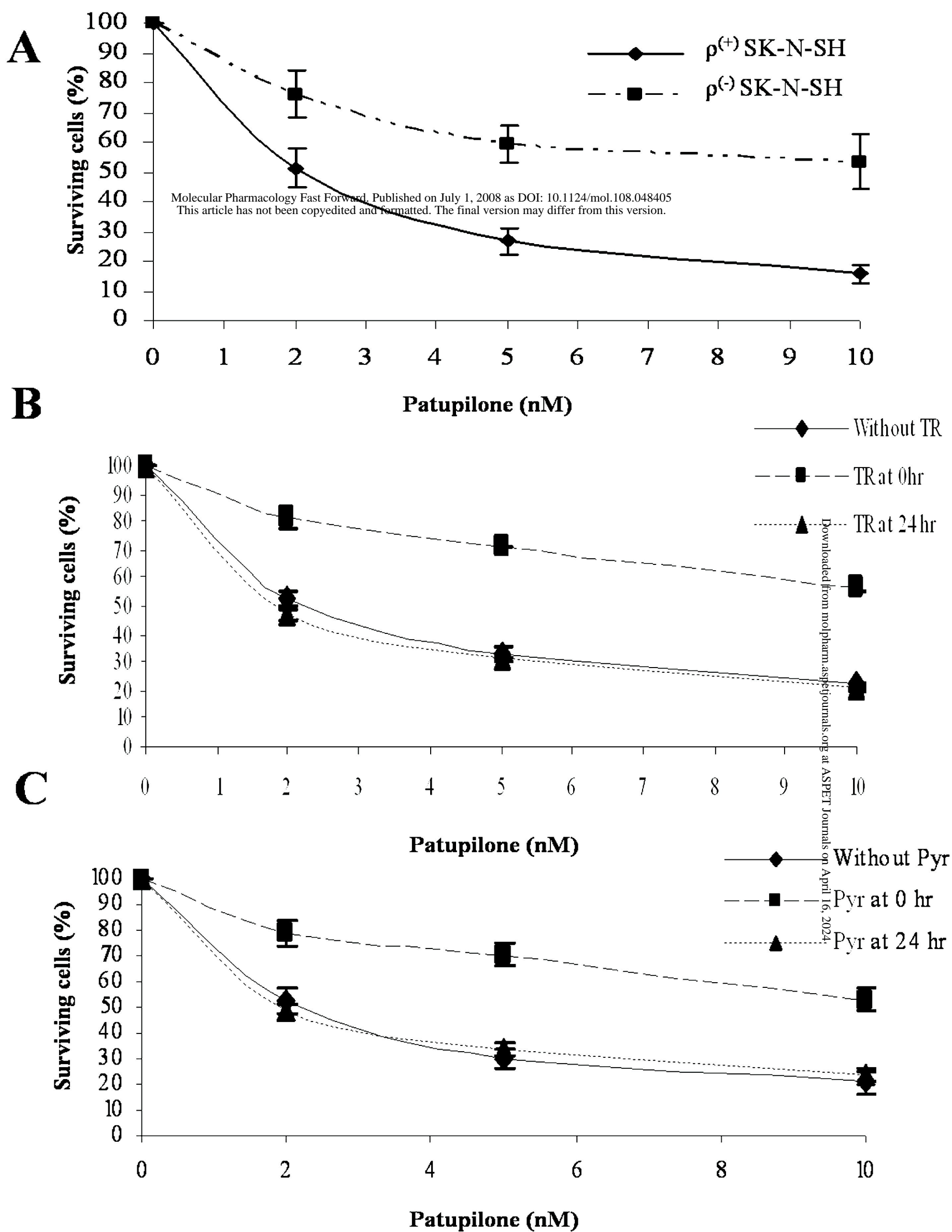


Figure 7

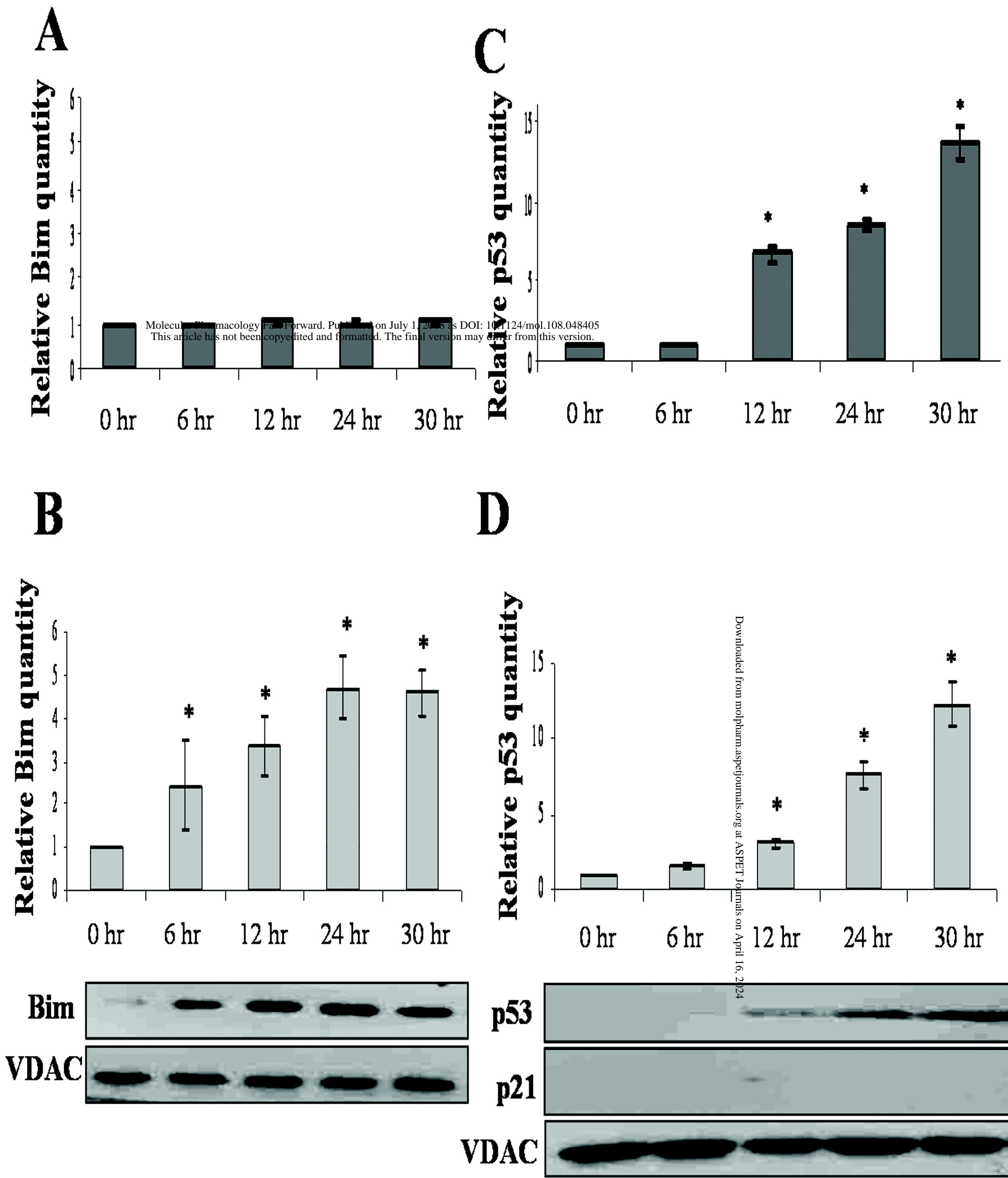
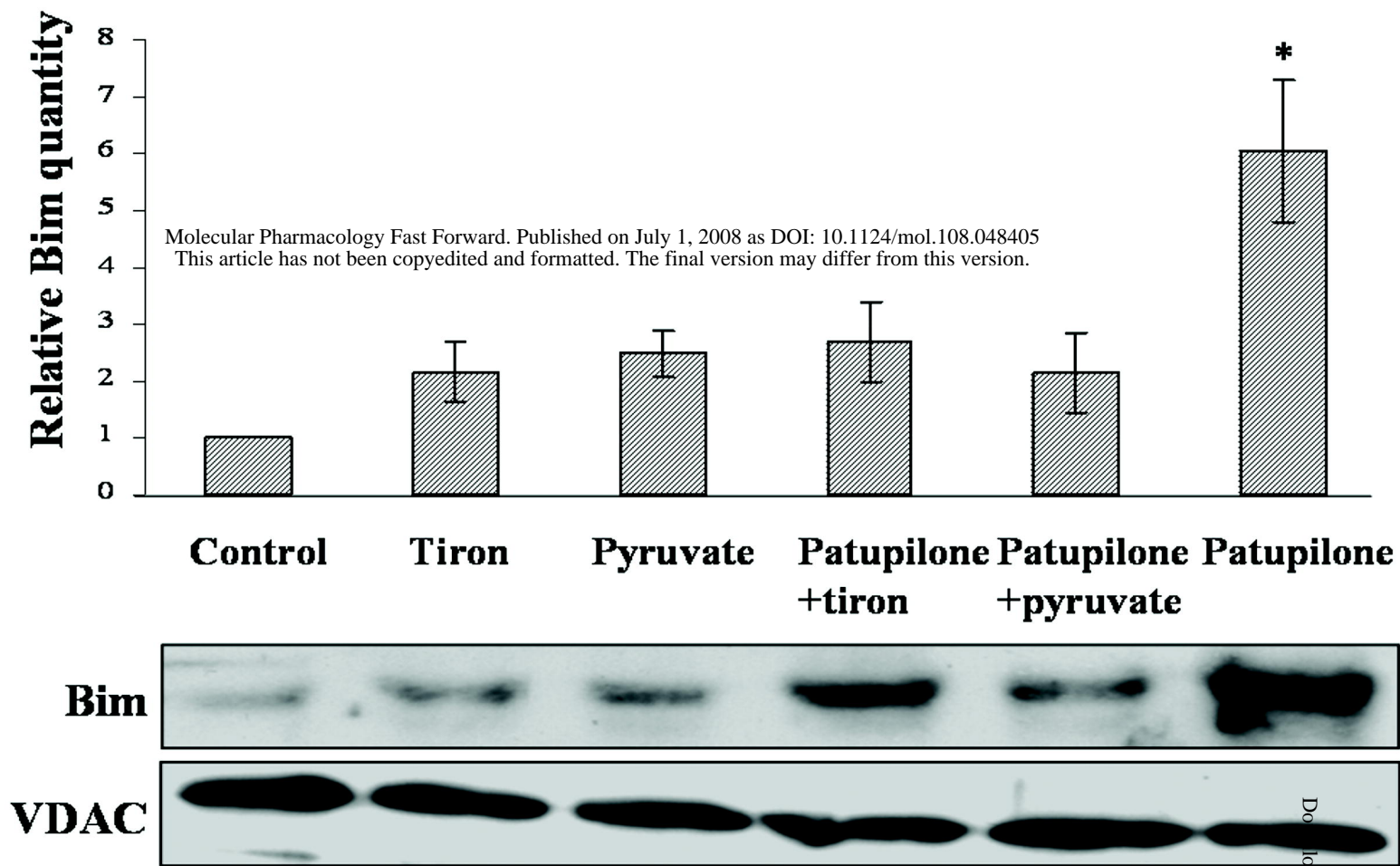
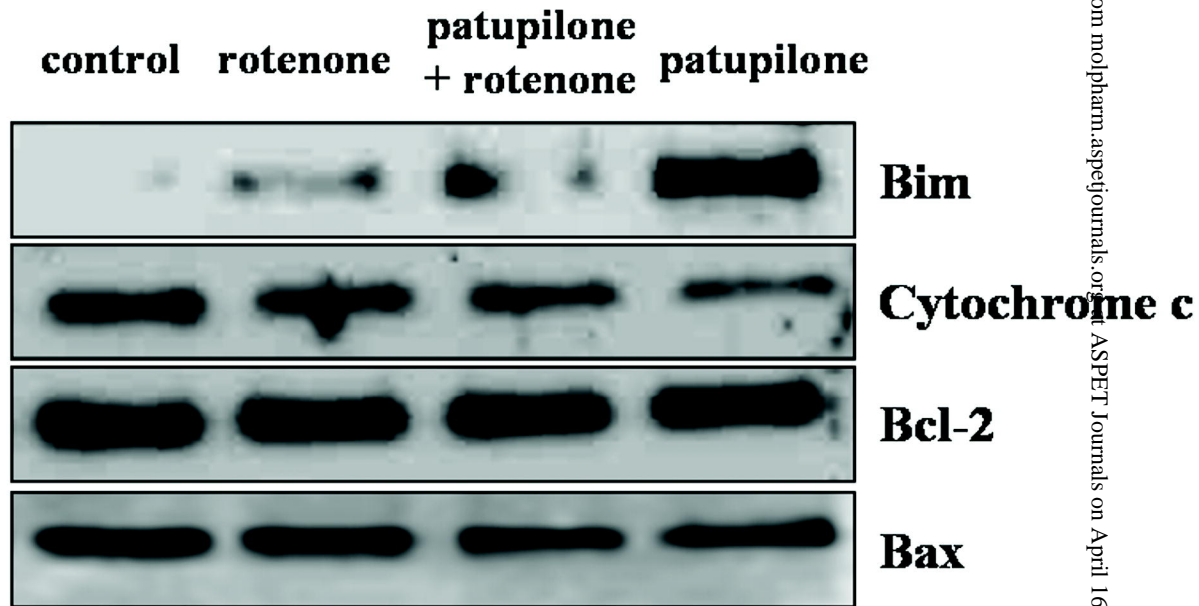
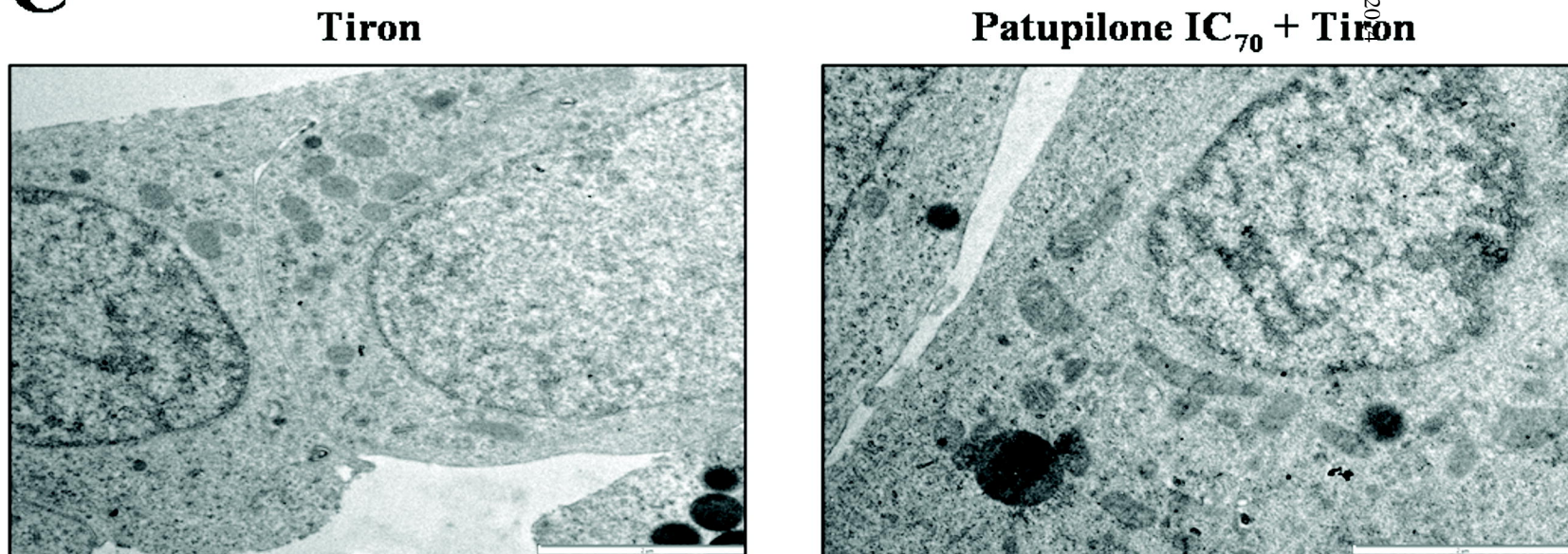


Figure 8

A**B****C****Figure 9**